HYDROLOGICAL PROCESSES
Hydrol. Process. **26**, 2745–2764 (2012)
Published online 29 November 2011 in Wiley Online Library
(wileyonlinelibrary.com) DOI: 10.1002/hyp.8328

Hydrologic response of a Hawaiian watershed to future climate change scenarios

Mohammad Safeeq[1]* and Ali Fares[2]

[1] *Department of Geosciences, Oregon State University, 104 Wilkinson Hall, Corvallis OR 97331, USA*
[2] *Department of Natural Resources and Environmental Management, University of Hawaii at Mānoa, 1910 East West Road, Honolulu HI 96822, USA*

Abstract:

The impact of potential future climate change scenarios on streamflow and evapotranspiration (ET) in a mountainous Hawaii watershed was studied using the distributed hydrology soil vegetation model (DHSVM). The hydrologic response of the watershed was simulated for 43 years for different levels of atmospheric CO_2 (330, 550, 710 and 970 ppm), temperature (+1.1 and +6.4 °C) and precipitation (±5%, ±10% and ±20%) on the basis of the Intergovernmental Panel on Climate Change (IPCC) AR4 projections under current, B1, A1B1 and A1F1 emission scenarios. Vegetation leaf conductance and leaf area index were modified to reflect the increase in CO_2 concentration. The relative departure of streamflow and ET from their levels during the reference scenarios was calculated on a monthly and annual basis. Results of this study indicate that the streamflow and ET are less sensitive to changes in temperature compared with changes in precipitation. However, temperature increase coupled with precipitation showed significant effect on ET and streamflow. Changes in leaf conductance and leaf area index with increasing CO_2 concentration under A1F1 scenario had a significant effect on ET and subsequently on streamflow. Evapotranspiration is less sensitive than streamflow for a similar level of change in precipitation. On the basis of a range of climate change scenarios, DHSVM predicted a change in ET by ±10% and streamflow between −51% and 90%. From the six ensemble mean scenarios for AR4 A1B, simulations suggest reduction in streamflow by 6.7% to 17.2%. These reductions would produce severe impact on water availability in the region. Copyright © 2011 John Wiley & Sons, Ltd.

KEY WORDS Climate Change; Streamflow; DHSVM; Hawaii

Received 14 March 2011; Accepted 5 September 2011

INTRODUCTION

Anthropogenic activities (e.g. burning of fossil fuels and coals) are changing the global climate (Hansen *et al.*, 2006) by increasing the concentration of the greenhouse gases especially methane, nitrous oxide and carbon dioxide (CO_2). The atmospheric CO_2 is expected to increase from its current concentration of approximately 330 ppm to between 550 and 970 ppm by 2100 (IPCC, 2007). Increased greenhouse gas concentrations are likely to raise the earth's mean temperature and influence precipitation and storm patterns as well as sea level (IPCC, 2007). However, broadly, the magnitude of these changes will depend on future anthropogenic activities as well as on the technological and economic development. Over the 21st century, the global average surface temperature has increased by approximately 0.6 °C and is projected to rise by an additional 1.1 to 6.4 °C (IPCC, 2007).

The historical trends in precipitation and air temperature on Hawaiian Islands have been extensively studied (Karl *et al.*, 1996; Chu and Chen, 2005; Giambelluca *et al.*, 2008; Timm and Diaz, 2008; Chu *et al.*, 2010). Timm and Diaz (2008) analysed the precipitation changes over the Hawaiian Islands during the late 21st century using the AR4 A1B emission scenario. From the downscaling of six global circulation models (GCM), Timm and Diaz (2008) concluded a 5%–10% reduction of wet season precipitation and 5% increase during the dry season. Using a linear trend analysis of observed air temperature and precipitation at Honolulu airport, Hawaii, Karl *et al.* (1996) reported an increase of the mean air temperature by 2.5 °C and 20% decrease in precipitation between 1900 and 1990. Since the 1980s, more frequent light precipitation and less frequent moderate and heavy precipitation have been observed in Hawaii (Chu *et al.*, 2010; Timm *et al.*, 2011). Using observed temperature across the Island of Oahu, Safeeq (2010) reported a 0.43 and 0.29 °C per decade increase in minimum and maximum air temperatures, respectively, during 1949–2007. At a longer (1905–2006) time scale, Giambelluca and Luke (2007) reported an increasing trend in the mean annual temperature between 0.12 and 0.23 °C per decade across the Hawaiian Island. Although the magnitude of change in temperature and precipitation varied temporally and spatially, the anticipated impact on the hydrology of mountainous Hawaiian watersheds cannot be disregarded.

Observed and anticipated changes in climate have significant implications on water resource management. Many studies have focussed on how climate variables such as temperature and precipitation will affect the watershed and global scale hydrologic cycle in the future

*Correspondence to: Mohammad Safeeq, Geosciences, Oregon State University, 104 Wilkinson Hall, Corvallis, OR 97331, USA.
E-mail: Mohammad.Safeeq@oregonstate.edu

(Arnell, 1999; Allen and Ingram, 2002; Ficklin *et al*., 2009). Regional scale changes in the seasonal distribution of precipitation (Groisman *et al*., 2004) and runoff (Milly and Dunne, 2001; Mishra *et al*., 2010) have already been observed. However, the magnitude and direction of change will largely depend on the geographic location, model used, climate change scenarios and the flow characteristic examined (Boorman and Sefton, 1997). Using the projection from the Hadley Centre climate model, Arnell (1999) projected the annual runoff increases in high-latitude regions, equatorial Africa and Southeast Asia and decreases elsewhere. The spatial variations in runoff sensitivity and its varying implications (Lettenmaier *et al*., 1999; Legesse *et al*., 2003; Labat *et al*., 2004) exemplify the need for site specific climate change investigations.

Anticipating changes in the hydrologic cycle is particularly important for regions with limited water supplies (Ficklin *et al*., 2009). Examining the sensitivity of hydrologic responses to climate across different physiographic regions is important to formulate appropriate water management policies for local response (Qi *et al*., 2009). The Hawaiian Islands are the most isolated oceanic Island group on earth and rely exclusively on precipitation and subsequent groundwater recharge for their fresh water needs (Mair and Fares, 2010a). Streams in Hawaii supply more than 50% of irrigation water and a fair amount of drinking water in some places (Oki, 2003). Groundwater aquifers supply 99% of Hawaii's drinking water and 50% of all fresh water used statewide (Gingerich and Oki, 2000). Since 1900, the population of Hawaii has increased approximately by eightfold (http://www.census.gov/). With increasing population over time, the demand for freshwater has significantly increased and expected to continue under the risk of climate change. For example, Wai'anae district can currently meet 50% of its water demand ($35\,204\,m^3\,day^{-1}$) with the local groundwater aquifer, and the rest is transferred from the neighbouring Pearl Harbor district (BWS, 2010).

In this study, the links between anticipated climate change and watershed scale hydrologic processes were studied to better understand the climate change impact on water resources in the region. The specific objectives of this research are (i) to perform a climate change sensitivity analysis using the distributed hydrology soil vegetation model (DHSVM) and (ii) to determine the relative role of changes in atmospheric CO_2, precipitation and temperature on Mākaha streamflow and evapotranspiration (ET). To our knowledge, this is the first attempt to assess the sensitivity of streamflow and ET to future climate change scenarios in a Hawaiian watershed.

MATERIALS AND METHODS

Description of study area

Climate change sensitivity assessment was performed in Mākaha watershed, located on the leeward coast of the Island of Oahu, Hawaii, USA (Figure 1). This watershed has an area of $13.84\,km^2$, an average slope of 66% and an elevation varying between 8 and 1227 m msl. Talus and basalt cover most of the areas along the steep valley walls, and non-calcareous sediments overlie the valley floor (Mink, 1978). On the basis of a 1:24 000 scale reconnaissance soil surveys (USDA-NRCS, 2008), 23% of the soil in the watershed is grouped as Tropohumult–Dystrandepts association (Figure 2A). Surface soil in Tropohumult–Dystrandepts association is mostly silty clay with textured subsoil and saprolite underneath. Rockland and rock outcrop constitutes 38% of the watershed, mostly the gulches and along the valley walls. The valley bottom of the watershed is composed of stony silty clay (15%), silt loam (10%), clay loam (5%), silty clay (3%), silty clay loam (4%) and mucky peat (~1%).

Land use/land cover is mostly dominated by dry evergreen forest (82%), grassland (7%) and shrubs (6%) with a small portion of palustrine forested wetland (<1%) near Mt. Ka'ala (Figure 2B).The remaining 4% of the watershed is occupied by open space urban developments, impervious roads and water bodies. In terms of vegetation, the watershed is largely occupied by non-native species such as strawberry guava (*Psidium cattleianum*), kukui (*Aleurites moluccana*), coffee (*Coffea arabica*), Christmas berry (*Schinus terebinthifolius*) and Java plum (*Syzygium cumini*). Some native tree species including Ōhi'a (*Metrosideros polymorpha*), A'ali'i (*Dodonaea viscosa*), koa (*Acacia koa*) and Lama (*Diospyros sandwicensis*) can also be found (Harman, 2006).

Rainfall is largely dictated by topography and the prevailing northeast trade winds. Average annual rainfall varies from 600 mm near the coast to more than 2000 mm at the crest (Giambelluca, *et al*., 1986). Approximately 70% of the normal precipitation falls during the wet season (also known as *ho'oilo* season) extending from November to April. Orographic lifting of moisture-laden northeast trade winds up the windward slopes (Giambelluca, 1986) and cyclonic rainfall produced by large-scale storm systems are the two principle rainfall-producing mechanisms in Hawaii (Giambelluca, 1983). Seasonal variation in rainfall on the leeward slopes causes higher rainfall gradient compared with the windward slopes where orographic effects are most pronounced during the summer (Chu and Chen, 2005). Over the Island of Oahu, the average monthly diurnal temperature range is very small (~7 °C) and remains nearly steady throughout the year (Safeeq, 2010). Large-scale atmospheric circulation processes, such as El Niño-Southern Oscillation (ENSO) and Pacific Decadal Oscillation, partially control the inter-annual and interdecadal variability in Hawaii rainfall, respectively (Chu and Chen, 2005).

Mākaha watershed lies within the marginal dike sector (60 dikes km^{-1}) of the northwest rift zone of the Wai'anae volcano (Takasaki and Mink, 1985). The natural placement of dikes in Mākaha watershed allows groundwater flux within dike compartments to move perpendicular to the Mākaha stream (Mair and Fares, 2010a). Mākaha stream cuts some of the dike-intruded high-level aquifers and

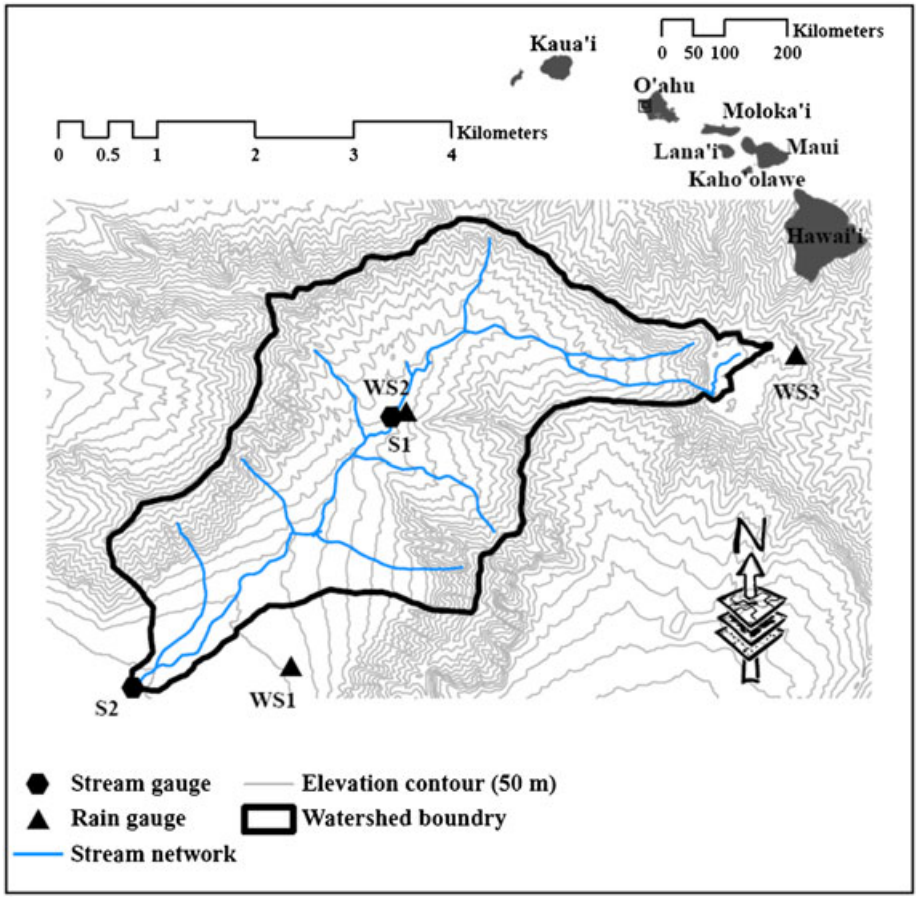

Figure 1. Study area with three long-term climate gauging stations (WS1, WS2 and WS3) and two streamflow monitoring stations (S1 and S2)

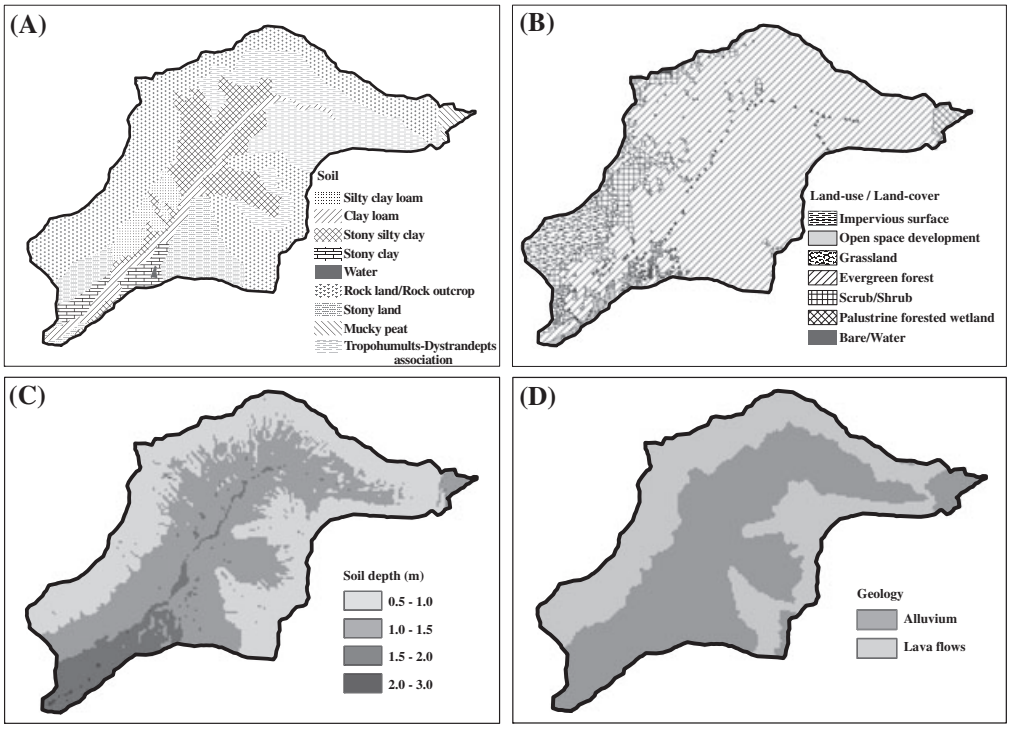

Figure 2. Spatially distributed (A) soil, (B) land use/land cover, (C) soil depth and (D) geology used during simulation

remains perennial in the upper part of the watershed (Mink, 1978). However, the length of the perennial portion of stream has decreased over time because of water resource development activities, including groundwater extraction wells, diversion ditches and gravity-fed tunnel (Mair and Fares, 2010a).

The hydrology of Mākaha watershed is strongly influenced by wet season rain. At gauge S1 (Figure 1), approximately 84% of the stream flow occurs during wet season. The total length of the main stream above gauge S1 is approximately 4.8 km with an average bed slope of 12.4% and an estimated time of concentration and time to peak are 0.41 and 0.38 hr, respectively (Wu, 1969). Higher watershed gradient and small time of concentration often cause flash flood downstream. Most of the streamflow comes from runoff, and the average baseflow index (ratio of baseflow to total flow volume) is only 0.28 (Mair and Fares, 2010a). There are currently eight groundwater pumping wells, one shaft and one 1283 m gravity-fed tunnel known as the Glover tunnel operating to supply irrigation and drinking water. Many of these extraction wells were brought online after 1991 to meet the increasing water demand. The Glover tunnel was built in 1945 and begins at an elevation of 171 m, extending from the mid-valley to within 300 m of stream gauge S1. An average outflow of 2800 $m^3 day^{-1}$ (0.20 $mm day^{-1}$) was recorded from the tunnel during 1949–1956 and 1961–1965 (Takasaki, 1971). As a result of these water-resource development, especially groundwater pumping (Mair and Fares, 2010a; Safeeq, 2010), significant decline in the Mākaha streamflow has been reported. Climate change might further exacerbate the ecological and hydrological balance of the watershed.

Description of DHSVM

DHSVM (Wigmosta *et al.*, 1994) is a physically based watershed-scale distributed hydrologic model. We selected this model because it was developed for high terrain mountainous watersheds. DHSVM has been used in addressing a variety of issues including streamflow forecasting (Yoshitani *et al.*, 2009; Zhao *et al.*, 2009), hydrologic effects of land management (Alila and Beckers, 2001; Thanapakpawin *et al.*, 2007) and climate change (Wiley and Palmer, 2008; Cuo *et al.*, 2009). The model computes water and energy balance at an applied spatial resolution and requires both spatially distributed (e.g. soil, vegetation, elevation and geology) and time series data (e.g. precipitation, temperature, wind speed, solar radiation and relative humidity) at each time step. A two-layer canopy model is used for ET; however, runoff is generated through saturation and infiltration excess mechanisms on the basis of a user-specified infiltration capacity. Saturated subsurface flow is modelled using a quasi three-dimensional routing scheme. DHSVM uses Muskingum–Cunge scheme for runoff routing through channel network. A detailed description of DHSVM and its governing equations can be found in the study of Wigmosta *et al.* (1994).

Model input data

DHSVM input parameters, for example, topography, soil, vegetation, geology and weather data, were prepared and are briefly detailed in the next section. A 10-m resolution digital elevation model (DEM) was obtained from the United States Geological Survey (USGS) (available at http://data.geocomm.com/dem/). Stream networks were generated from a10-m resolution DEM using ArcInfo (ESRI, 2006). We adjusted the critical source area iteratively until a reasonable agreement between the DEM-generated stream network and the digital stream (both perennial and intermittent) network on the basis of the USGS hydrography layer (available at http://hawaii.gov/dbedt/gis/download.htm) was achieved. A critical source area of 0.25 km^2 resulted in a better agreement between the two aforementioned stream network layers. Distributed soil data were obtained from a 1:24 000 scale Soil Survey Geographic (SSURGO) database (USDA-NRCS, 2008) and grouped on the basis of texture classes (Figure 2A). Soil depth (Figure 2C) was generated on the basis of the DEM using ArcInfo subroutines provided with DHSVM. The DEM-generated soil depth was verified against field measurements of soil depth at the six monitoring locations across the watershed. Soil physical properties for each class were obtained from Verger (2008) and Yamamoto (1963).

Land use/land cover was defined on the basis of a 2.4-m resolution land use survey data obtained from the National Oceanic and Atmospheric Administration Coastal Change Analysis Program (C-CAP) (USDC-NOAA, 2005). Vegetation parameters required by DHSVM were mostly derived from the literature (Dickinson *et al.*, 1986; Canadell *et al.*, 1996; Cosgrove and Rodell, 1999; Breuer *et al.*, 2003). The leaf area index (LAI) for evergreen forest was based on site specific plant area index measurements (Mair and Fares, 2010b). The value of LAI rain multiplier was estimated using a maximum canopy storage capacity of 3.0 mm (Safeeq, 2010), an average LAI of 4.0 and a canopy cover of 100%. However, during the calibration, we further adjusted the LAI rain multiplier to match a canopy interception value equals to 30% the gross rainfall (Safeeq, 2010).

Sub-daily (3 hr) temporal resolution meteorological input data (precipitation, air temperature, wind speed, relative humidity and long- and short-wave solar radiation) were prepared at three long-term weather monitoring stations. These gauges have been operated by the USGS (WS2) and the National Climatic Data Center (WS1 and WS3); they are located within and/or in a proximity of the study area (Figure 1). Hourly precipitations were obtained at gauges WS1, WS2 and WS3 for the period of 1967–2009; then they were aggregated to 3 hr time step. At WS2 gauge, there were only records of daily precipitations during the periods of 1967–1993 and 1996–1999. These data were disaggregated into hourly values using the diurnal method as described by Safeeq and Fares (2011). The missing values of precipitations were estimated using the normal ratio method (Mair and Fares, 2010a). We also corrected the daily precipitation at gauge WS2 for tree catch (Mair and Fares, 2010c) using the double mass analysis between WS2 and WS3. Daily air temperature, wind speed and relative humidity were spatially interpolated from nearby Western Regional Climate Center gauges (available at http://www.wrcc.dri.edu/index.html) as

described by Safeeq (2010). To run DHSVM at 3 hr time step, we disaggregated daily air temperatures and wind speeds using a sine and a cosine model, respectively (Safeeq and Fares, 2011).

We used the monthly gridded precipitation data (Giambelluca *et al.*, 1986) to spatially distribute the 3-hr precipitation. Both temperature and precipitation were adjusted with positive and negative lapse rate with elevation, respectively. We estimated the lapse rates on a monthly basis using long-term observed precipitation and temperature data to maintain the seasonal variability. Hourly short-wave and long-wave solar radiations were calculated using the methods of Bristow and Campbell (1984) and Burman and Pochop (1994), respectively. Daily streamflow data for the 1967–2009 period at gauge S1 were obtained from the USGS. The reader is referred to Safeeq (2010) for a detailed description of the methods used to translate the climate data available at different temporal resolutions from the different gauges into a 3-hr forcing input for DHSVM.

DHSVM calibration and validation

Historic streamflow record at gauge S1 (Figure 1) between 1971 and 1990 were split into two equal periods of 10 years. DHSVM was calibrated with 1971–1980 data and validated with 1981–1990 data using the daily observed streamflow. The period after 1990 was excluded from the model calibration and validation to minimise the influence of water resource development on measured streamflow (Mair and Fares, 2011). The model was run at a 3-hr time step; simulated streamflow was aggregated into daily values to evaluate the model performance. During the model sensitivity analysis, we iteratively adjusted the value of one parameter at a time until a reasonable agreement was achieved between daily observed and simulated streamflow. In addition to calibrating against the observed streamflow data, DHSVM parameters (LAI, albedo and leaf conductance) were also adjusted so that the simulated ET would be between 51% and 54% of the gross rainfall (Giambelluca and Oki, 1987; Giambelluca *et al.*, 2009) while canopy interception would account for 30% of the gross rainfall (Safeeq, 2010). We were unable to calibrate the model against ET at a finer time scale (e.g., daily, weekly) because of the lack of the long-term daily or monthly site specific ET and canopy interception data. The final values of the vegetation and soil parameters achieved at the end of the calibration phase are given in Tables I and II, respectively.

DHSVM performance evaluation

The accuracy of DHSVM in simulating daily streamflow was evaluated using the coefficient of efficiency (E) (Nash and Sutcliffe, 1970), the correlation coefficient (R), the ratio of root mean squared error to observations standard deviation (RSR) and the model overestimation bias in percentage (PBIAS) (Gupta *et al.*, 1999). These accuracy indicators are defined as follows:

The coefficient of efficiency:

$$E = 1.0 - \frac{\sum_{i=1}^{N}(O_i - S_i)^2}{\sum_{i=1}^{N}\left(O_i - \ddot{O}\right)^2} \tag{1}$$

The correlation coefficient:

$$R = \frac{N\sum_{i=1}^{N}S_iO_i - \sum_{i=1}^{N}S_i\sum_{i=1}^{N}O_i}{\sqrt{N\sum_{i=1}^{N}O_i^2 - \left(\sum_{i=1}^{N}O_i\right)^2}\sqrt{N\sum_{i=1}^{N}S_i^2 - \left(\sum_{i=1}^{N}S_i\right)^2}} \tag{2}$$

The model overestimation bias in percentage:

$$\mathrm{PBIAS}(\%) = \frac{100 \times \sum_{i=1}^{N}(O_i - S_i)}{\sum_{i=1}^{N}(O_i)} \tag{3}$$

The ratio of root mean squared error to observations standard deviation:

$$\mathrm{RSR} = \frac{\sqrt{\sum_{i=1}^{N}(O_i - S_i)^2}}{\sqrt{\sum_{i=1}^{N}\left(O_i - \ddot{O}\right)^2}} \tag{4}$$

where O_i, S_i and $\ddot{O}$ are the measured, simulated and mean of measured values, respectively. N is the total number of data points in the simulation. E can take any value from minus infinity to 1; R and RSR vary between 0 and 1. However, PBIAS varies from 100 to negative infinity. A value of E more than 0.35 and less than 0.50 was considered an indicator of average performance; however, a value between 0.50 and 0.70 indicates a good performance, and a value greater than 0.70 indicates a very good performance. Similar thresholds for E were also suggested by other researchers (Mishra *et al.*, 2010; Oleson *et al.*, 2008). The model performance was considered as good if R was greater than 0.8 and very good if R was greater than 0.90. On the basis of RSR, the model performance is considered satisfactory if $\mathrm{RSR} \leq 0.70$, good if $\mathrm{RSR} \leq 0.60$ and very good if $\mathrm{RSR} \leq 0.50$. Values of PBIAS indicate the model's overprediction ($\mathrm{PBIAS} < 0$) or underprediction ($\mathrm{PBIAS} > 0$) of streamflow, where a value of 0 corresponds to a perfect prediction. The model performance is considered very good if the value of PBIAS is less than 10%, good if PBIAS is between 10% and 15% and satisfactory for values between 15% and 25%. Along with observed and simulated daily hydrograph, annual cumulative total streamflow, direct runoff and baseflow during the dry season (May–October), wet season (November–April) and on annual (January–December) basis were also compared.

Climate change scenarios

In this study, a total of 24 climate change scenarios (Table III) were generated on the basis of the IPCC Special

Table 1. Final values of DHSVM vegetation parameters at the end of the calibration phase

Vegetation parameters	Overstory[a]	Understory	Open shrub	Grassland
Impervious fraction (%)	<0.5	0	0	0
Fractional coverage[b]	0.9	–	–	–
Hemi fractional coverage[b]	0.9	–	–	–
Trunk space[b]	0.5	–	–	–
Aerodynamic attenuation[b]	2 ± 0.5	–	–	–
Radiation attenuation[b]	0.15 ± 0.05	–	–	–
Height (m)[c]	20 ± 4	1.5	3	0.5
Monthly LAI[c]	4.5 ± 0.25	1.6 ± 0.5	2.9 ± 1.3	0.5
LAI multiplier for rain (m)[d]	0.0008	0.0008	0.0008	0.0008
Maximum resistance ($s\,m^{-1}$)[d,e]	5000	3000	600	600
Minimum resistance ($s\,m^{-1}$)[d,e]	666.6 ± 150	200	178	178
Moisture threshold[d]	0.32–0.28	0.28	0.28	0.33
Vapor pressure deficit (Pa)[b]	4000	4000	4000	4000
Critical light level *R*pc ($W\,m^{-2}$)[b]	0.108	0.108	0.108	0.108
Monthly albedo[d]	0.13 ± 0.02	0.12	0.12	0.19
Root zone depth (m)[d]	0.75–2.0	0.35–1.1	0.35	0.35
Root fraction in layers 1, 2 and 3[d]	0.6, 0.3, 0.1	0.6, 0.4, 0.0	0.6, 0.4, 0.0	0.6, 0.4, 0.0

[a] Evergreen forest and palustrine forested wetland
[b] Model default
[c] Based on measured values at three locations (Mair and Fares, 2010b)
[d] Initial values are either model default or based on literature (Stratton, *et al.* 2000; Cordell, *et al.*, 1998; Santiago, *et al.* 2000; Alves de Sena, *et al.*, 2007)
[e] Modified parameters during calibration

Table 2. Final values of DHSVM soil parameters at the end of the calibration

Parameter	Soil layer	Soil type							
		SCL	CL	SSC	SC	RL/RO	SL	MP	Tp-D
Fraction of study area (−)		0.04	0.05	0.15	0.03	0.38	0.1	0.01	0.23
Bulk density ($kg\,m^{-3}$)	1	695	695	692	750	684	684	600	687
	2	750	750	760	960	742	742	612	742
	3	895	895	901	1050	950	950	650	901
Porosity (−)	1	0.66	0.645	0.675	0.725	0.666	0.668	0.77	0.72
	2	0.65	0.636	0.655	0.695	0.615	0.632	0.77	0.69
	3	0.645	0.616	0.645	0.693	0.605	0.632	0.77	0.65
Field capacity (−)	1	0.47	0.462	0.42	0.45	0.411	0.452	0.5	0.44
	2	0.479	0.465	0.425	0.455	0.415	0.463	0.52	0.455
	3	0.479	0.472	.432	0.46	0.425	0.467	0.54	0.464
Wilting point (−)	1	0.3	0.32	0.32	0.32	0.33	0.36	0.36	0.32
	2	0.32	0.28	0.33	0.33	0.34	0.32	0.36	0.32
	3	0.32	0.28	0.33	0.29	0.36	0.32	0.36	0.32
Maximum infiltration capacity ($10^{-3}{\cdot}m\,s^{-1}$)		0.30	0.10	0.10	1.00	0.40	0.80	7.40	8.81
Exponential decay of lateral K_{sat} (−)[a]		2.15	2.12	3.15	3.25	4.15	2.35	0.5	3.1
Lateral K_{sat} ($10^{-6}{\cdot}ms^{-1}$)		5.12	5.17	10.74	8.33	9.50	6.50	35.00	8.23
Vertical K_{sat} ($10^{-6}{\cdot}ms^{-1}$)	1	0.42	0.42	3.70	0.42	6.13	4.23	8.41	7.41
	2	0.23	0.23	2.67	0.22	4.15	3.23	8.41	6.11
	3	0.04	0.04	0.70	0.02	1.13	1.02	8.41	5.40

SCL, silty clay loam; CL, clay loam; SSC, stony silty clay; SC, stony clay; RL/RO, rock land/rock outcrop; SL, stony land; MP, mucky peat; Tp-D, Tropohumult–Dystrandepts association.
[a] Saturated hydraulic conductivity

Reports on Emission Scenarios (IPCC, 2001), local trend analysis and GCM downscaling (Timm and Diaz, 2008). On the basis of the IPCCs projections of green house gas emission for the 21st century, atmospheric concentration of CO_2 is expected to increase between 550 (B1 emission scenario) and 970 ppm (A1F1 emission scenario) from its current concentration of 330 ppm. The two extreme scenarios represent a future world of a very rapid economic growth (A1F1 emission scenario—970 ppm) or a future world with low economic growth and fossil fuel independency (B1 emission scenario—550 ppm). To bracket the range of changes in precipitation over the Hawaiian Islands, four arbitrary precipitation scenarios with respect to the current level (i.e. 0%, ±5%, ±10% and ±20%) were selected. Two additional precipitation-based scenarios were generated on the basis of six GCM

Table 3. Climate change sensitivity scenarios simulated using DHSVM based on the current (white), B1 (light gray), A1B (orange) and A1F1 (dark gray) emission scenarios

Scenarios	CO_2 Emission (ppm)	Temperature (°C)	Precipitation (%)
Reference	330	0	0
1	330	1.1	0
2	330	6.4	0
3	330	0	-5
4	330	0	-10
5	330	0	-20
6	330	0	5
7	330	0	10
8	330	0	20
9	550	1.1	0
10	550	1.1	-5
11	550	1.1	-10
12	550	1.1	-20
13	550	1.1	5
14	550	1.1	10
15	550	1.1	20
16	970	6.4	0
17	970	6.4	-5
18	970	6.4	-10
19	970	6.4	-20
20	970	6.4	5
21	970	6.4	10
22	970	6.4	20
23	710	0	-5% in wet and +5 % in dry season
24	710	0	-10% in wet and +5% in dry season

predictions for Hawaii under AR4 A1B emission scenario. Temperature-based scenarios were generated by increasing the temperature by 1.1 and 6.4 °C. All the climate change scenarios were generated using the 'delta method' (Hamlet and Lettenmaier, 1999) on observed precipitation and air temperature data at WS1, WS2 and WS3 between water years 1967 and 2009. Average monthly precipitations were increased or decreased in a relative term with a value of one meaning there is no change and a value of 1.05 meaning a 5% increase in precipitation compared with historical data. Changes in air temperature were made by adding the required 1.1 or 6.4 °C to observed temperature.

The complex and nonlinear forest–atmosphere interactions can dampen or amplify the anthropogenic climate change (Bonan, 2008). An increase in CO_2 concentration not only causes increases in air temperature but also will result in a reduction of leaf stomatal conductance (Saxe *et al*., 1998; Medlyn *et al*., 2001; Wullschleger *et al*., 2002) and an increase in LAI because of enhanced photosynthesis (Pritchard *et al*., 1999; Wand *et al*., 1999). Doubling of CO_2 concentration could decrease the stomatal conductance by 40% in crops (Morison, 1987) and 21% (Medlyn *et al*., 2001) to 23% (Field *et al*., 1995) in tree species. We adjusted the stomatal conductance of all vegetation classes in the model using a similar approach to that used in SWAT (Arnold *et al*., 1998) model based on the following equation (Easterling *et al*., 1992):

$$g_{CO_2} = g \times \left[1.4 - 0.4 \times \left(\frac{CO_2}{330}\right)\right] \quad (5)$$

where g_{CO2} is the modified conductance to reflect the increased CO_2 effects, g is the conductance without the effect of CO_2, CO_2 is the increased CO_2 concentration level and 330 represents the current atmospheric CO_2 concentration. Pritchard *et al*. (1999) reported an increase of LAI by 37% in crop species, 15% in wild non-woody species and 14% in tree species. Similar to Eckhardt and Ulbrich (2003), we used a smaller increase (7%) in LAI with doubling of CO_2 concentration for all vegetation types.

Although, many studies mentioned earlier confirm the effect of elevated atmospheric CO_2 on plant LAI and leaf conductance, the process will be dynamically opposed to a step change (adopted in this study) and may take few years to decades before any significant change in LAI or leaf conductance can be seen. In addition, the elevated CO_2 can alter plant growth, biomass and chemical composition of plant tissues. However, all of these changes will depend on the hydrologic feedback between vegetation, soil and atmospheric conditions (Niyogi and Xue, 2006). We want to show how potential changes in LAI and leaf conductance might influence ET and streamflow keeping in mind the uncertainty and complex

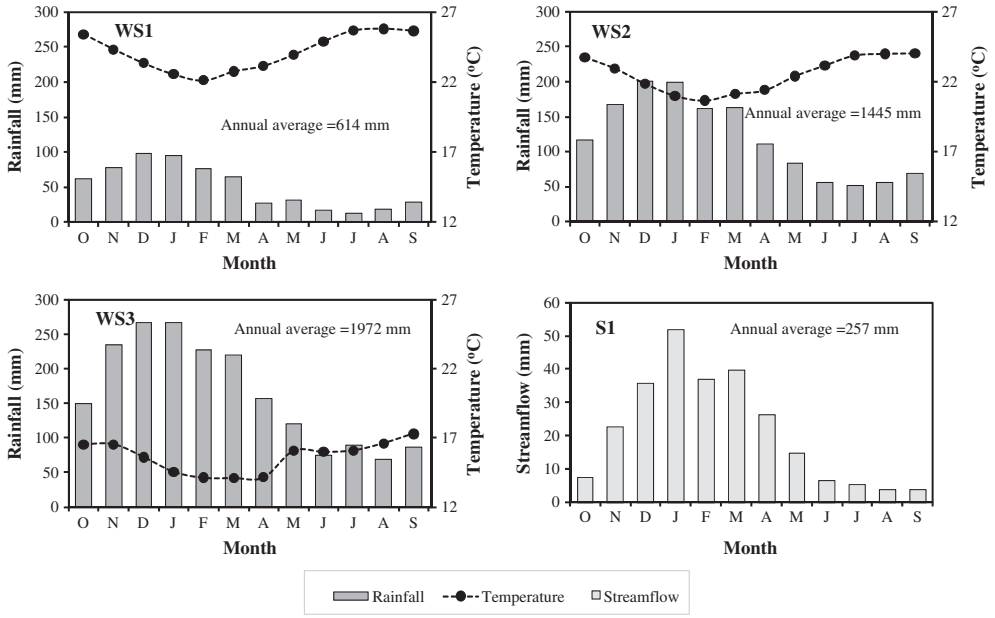

Figure 3. Climographs of mean monthly precipitation, average temperature and streamflow for Mākaha watershed. Temperatures at WS2 and WS3 were estimated from WS1 and nearby Western Regional Climate Center Remote Automated Weather Stations

nonlinear response (Drake *et al*., 1997; Long *et al*., 2004; Taub, 2010) of vegetation to elevated atmospheric CO_2 concentration. Because greenhouse gasses are the primary driver for projected changes in temperature and precipitation, it is important to consider the direct effect of CO_2 on vegetation which can substantially influence the surface hydrological processes (Alo and Wang, 2008). We will explicitly address the relative hydrologic effect of potential changes in precipitation, temperature and CO_2.

Climate change scenarios were simulated using DHSVM for a 43-year period (1967–2009) after adjusting precipitation and temperature. Scenarios with 550 and 970 ppm CO_2 emissions were repeated after adjusting the LAI and leaf conductance. Other climate variables (i.e. solar radiation, wind speed and relative humidity) were kept constant for all scenarios. Simulation results were then summarised on a monthly, seasonal and annual basis and were compared with the reference scenario. Two-

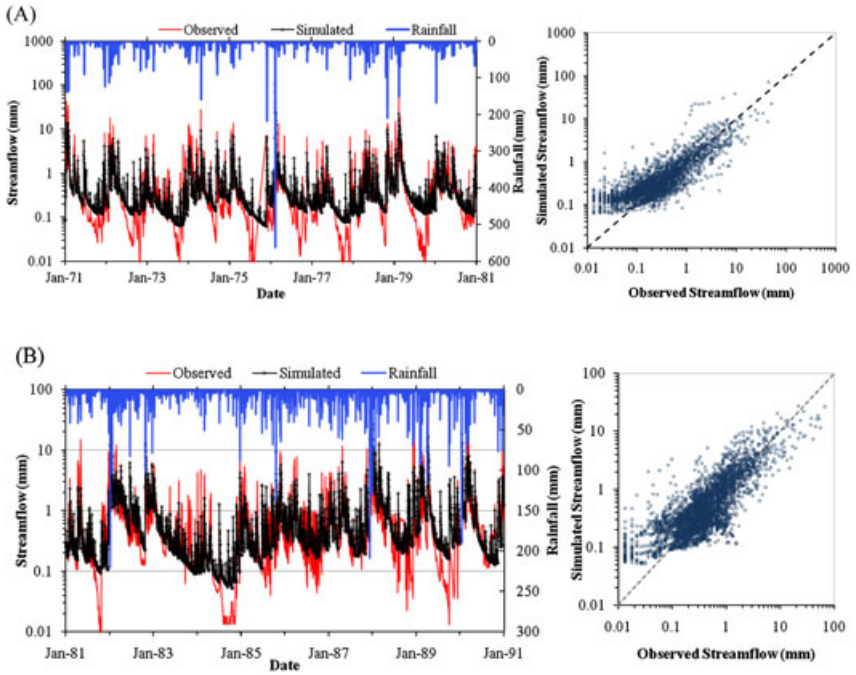

Figure 4. Hydrograph of observed and simulated streamflow during (A) calibration and (B) validation periods at the USGS stream gauge S1. Corresponding watershed average daily rainfall is shown on the secondary axis. The figure on the right panels of A and B are plots of observed and simulated streamflow along with the 1:1 line.

sample *t*-tests were used to compare the selected climate scenario with the reference scenario.

RESULTS

Climographs showing the mean monthly precipitation, average temperature and streamflow for Mākaha watershed between 1967 and 2009 are presented in Figure 3. Rainfall is largely dictated by topography, and a strong coast to mountain crest rainfall gradient exists between the gauge WS1, WS2 and WS3. Average annual rainfall at gauge WS1 and WS2 are only 31% and 73% of the total rainfall at WS3, respectively. In addition, the variance in the mean monthly precipitation increased from WS1 to WS3, indicating greater seasonal variability in monthly precipitation at higher elevation. The streamflow correlates well with the rainfall; this correlation is high during the wet season and low during the dry season. In contrast to precipitation and streamflow, seasonal air temperature amplitudes were small ($< 5\,^{\circ}C$).

DHSVM calibration

Observed and simulated daily streamflow hydrographs shol reasonable agreement during the calibration period (Figure 4A). DHSVM underpredicted the peak flows during high rainfall events and overpredicted the low flows (<0.1 mm) during the dry season. The ability of the model to capture the dry season baseflow was improved after adjusting the soil depth, plant available water and lateral saturated hydraulic conductivity. Cuo *et al.* (2006) and Thanapakpawin *et al.* (2007) reported similar behaviour of DHSVM; it does not simultaneously match very well both the stream peak flow and the baseflow. Beckers and Alila (2004) attributed these tradeoffs between accurate simulation of peak flow and baseflow to the poor representation of preferential flow in the model. Preferential pathways in the form of macropores, fractures and root holes facilitate the quick movement of water out of the simulated system. Thus, no effort was made to match low flows on the cost of underestimating high flows because the contribution of the former to the total monthly and annual flow was insignificant ($< 1\%$). Notably, a substantial portion of the stream base flow ($0.15\,mm\,day^{-1}$) has been captured by Glover tunnel since its inception (Takasaki, 1971). We were unable to correct the measured flow at S1 because of the lack of the long-term flow measurement from the tunnel. However, two short-term measurements from the tunnel during 1949–1956 and 1962–1965 (Mair and Fares, 2011) indicate that a new hydrologic equilibrium could have been reached before 1971(year after which model was calibrated and validated). Hence, the transient effect of the Glover tunnel on stream baseflow above gauge S1 (Figure 1) can be considered negligible.

Simulated annual streamflow matches reasonably well with the measured streamflow except for 1976 during which DHSVM overpredicted the total streamflow because of a 1-day rainfall storm that from the tunnel 556 mm of rain (Figure 4A). DHSVM underpredicted the total streamflow during the wet season and overpredicted it during the dry season (Figure 5). There is a reasonable agreement between the simulated and the observed annual and dry season direct runoff; however, the model underpredicted the direct runoff during the wet season. The performance of DHSVM in simulating the baseflow during the dry season was mixed with slight overprediction during 6 years and matched well during the remaining 4 years (1973, 1977, 1978 and 1980). The simulated baseflow of the wet season was comparable with the observed baseflow except for 1976, the year with that single high rainfall event in February, when DHSVM overpredicted baseflow (Figure 5).

The model performance over the entire calibration period is considered 'satisfactory' to 'good' on the basis of the four performance criteria used ($R = 0.83$, $E = 0.68$, $PBIAS = 0.24$ and $RSR = 0.57$). Similarly, its yearly performance is also considered overwhelmingly 'good' on the basis of the *R*, *E* and RSR indicators. On the yearly basis, DHSVM performance is considered 'good' for most of the years if we use *R*, *E* and RSR criteria. However, it has a mixed performance based on the PBIAS criteria (Table IV).

Validation of DHSVM

There is a better agreement between observed and simulated streamflow hydrographs during the validation period compared with the calibration (Figure 4B), which can be attributed in part to a slightly more uniform precipitation during this period. The wet and dry season rainfall during the validation period were 4% and 31% higher compared with that of the calibration period, resulting in a relatively uniform rainfall within the year. This can be attributed to the fact that Pacific Decadal Oscillation, which is negatively correlated with precipitation in Hawaii (Chu and Chen, 2005), was in a positive phase during the model validation period. DHSVM performance was poor during the late part of 1983 and early part of 1984 because of an extreme drought. The period 1971–1986 had a statewide drought resulting in a significantly lower 1-, 7- and 30-day average minimum streamflow (Oki, 2004) at gauge S1.

DHSVM slightly underpredicted the annual total streamflow (Figure 5) except for the years with extreme rain events during which the model overpredicted the total streamflow. It underpredicted the direct runoff of all magnitudes and overpredicted the baseflow during wet years. We compared observed and simulated hydrographs on individual event basis (i.e. February 1976 event) to further investigate this tradeoff between overland flow and baseflow during wet years. A comparison of event-based hydrographs indicates that DHSVM significantly underpredicted the peak flow and overpredicted the baseflow during the flow recession portion of the hydrograph. This indicates that during high-intensity rainfall, the overland flow is not accurately represented

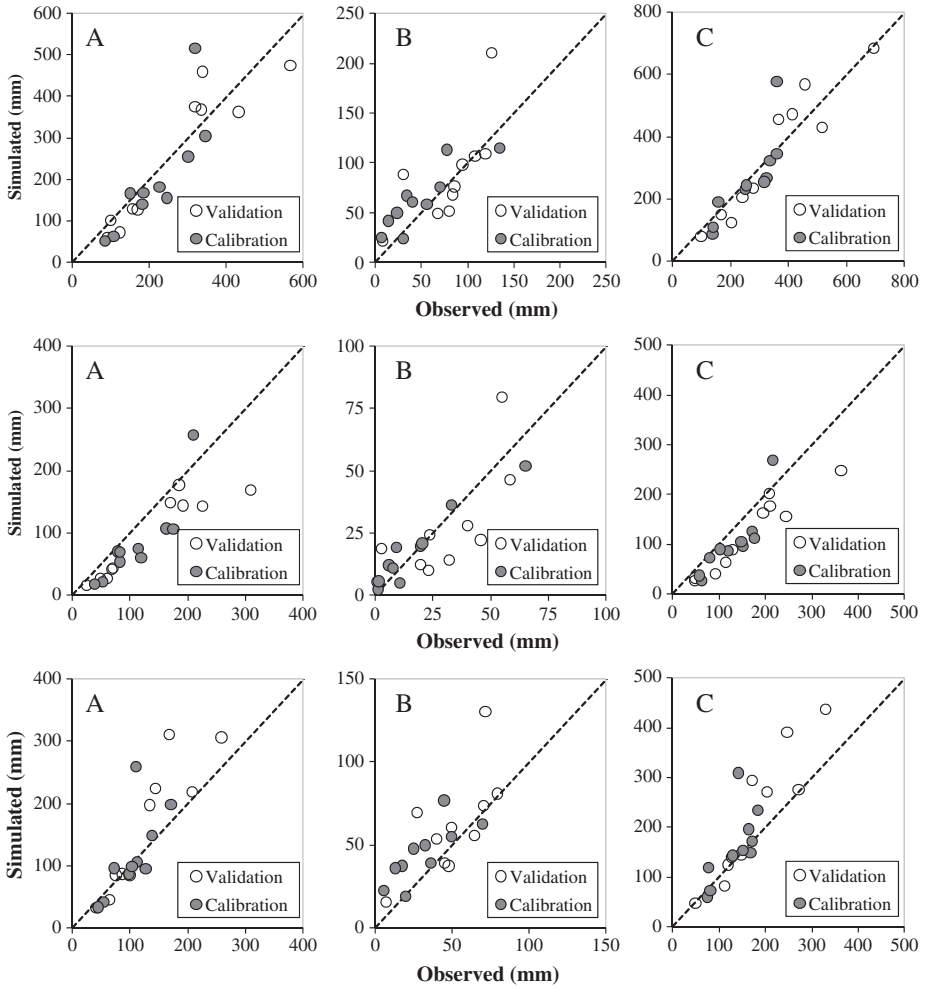

Figure 5. Comparison between observed and simulated streamflow components, baseflow (bottom), direct runoff (centre) and total flow (top) during the (A) wet season, (B) dry season and (C) entire year (the dotted line is the 1:1 line)

by the static user-specified infiltration capacity implemented in DHSVM. Because infiltration rate depends on the degree of saturation of the soil, a dynamic infiltration capacity would probably be more accurate under these conditions.

The mean daily simulated streamflow values during each year of the model validation period were in agreement with their corresponding mean daily observed flow values (Table IV). On an annual basis, the values of R varied between 0.75 and 0.98; however the coefficient of efficiency ranged between 0.41 and 0.78. The values of RSR were in the ranges of 0.46 to 0.77. Streamflow was overestimated during 1987–1989 (PBIAS < 0) and underpredicted during the rest of the period. However, over- and/or underpredictions were satisfactory (PBIAS < 25) except for 1981. The model performance is considered satisfactory on the basis of the values of the four indicators R (0.86), E (0.86), PBIAS (0.81) and RSR (0.68).

The mean monthly observed and simulated streamflow and ET values for the combined period (calibration and validation) were plotted to test if the model captures the month-to-month variability. Overall, the model does a reasonable job of reproducing the month-to-month variability in total streamflow, baseflow, direct runoff and ET (Figures 6A–6D). The over- and/or underprediction of mean January and February flows were primarily associated with few extreme rain storms as discussed earlier. Two-sample Kolmogorov–Smirnov test results showed no significant difference ($D = 0.094$, $p = 0.58$) between observed and simulated wet season monthly streamflow. However, the null hypothesis of no significant difference between dry season observed and simulated monthly streamflow was rejected ($D = 0.23$, $p = 0.01$). Monthly ET values were higher during the wet season compared with the dry season, which can be mostly attributed to higher interception losses rather than higher soil moisture. Giambelluca *et al.* (2009) also reported similar seasonal distribution of ET and found no correlation with soil moisture.

Comparison with previous ET and recharge estimates

Because DHSVM was only calibrated against daily observed streamflow and long-term average ET, we compared the simulated water balance components with previous studies in Hawaii (Table V). The simulated annual ET represents 56% of the annual rainfall for Mākaha watershed, which is in the range of what was reported for

Table 4. DHSVM performance statistics during calibration and validation at gauge S1

	Year	Mean daily flow		Model performance statistics			
		Observed (mm)	Simulated (mm)	*R*	*E*	*PBIAS* (%)	*RSR*
Calibration	1971	0.92	0.88	0.78	0.53	4.02	0.68
	1972	0.68	0.63	0.86	0.63	7.76	0.61
	1973	0.38	0.23	0.69	0.46	37.82	0.73
	1974	0.89	0.73	0.82	0.55	17.36	0.67
	1975	0.43	0.52	0.92	0.82	-21.24	0.42
	1976	0.98	1.58	0.87	0.72	-60.85	0.53
	1977	0.38	0.30	0.82	0.69	22.41	0.56
	1978	0.86	0.70	0.90	0.78	19.41	0.47
	1979	0.98	0.95	0.86	0.69	3.74	0.55
	1980	0.70	0.66	0.76	0.54	4.39	0.68
	Entire period	0.72	0.72	0.83	0.68	0.24	0.57
Validation	1981	0.56	0.34	0.86	0.41	39.82	0.77
	1982	1.90	1.88	0.90	0.48	0.97	0.72
	1983	0.46	0.41	0.93	0.77	10.78	0.48
	1984	0.27	0.22	0.85	0.78	19.00	0.46
	1985	0.76	0.64	0.82	0.62	15.46	0.62
	1986	0.66	0.56	0.75	0.61	15.52	0.63
	1987	1.13	1.30	0.98	0.45	-14.60	0.74
	1988	1.25	1.55	0.97	0.60	-24.38	0.63
	1989	1.00	1.25	0.98	0.59	-24.84	0.64
	1990	1.41	1.18	0.94	0.51	16.54	0.70
	Entire period	0.94	0.93	0.86	0.54	0.81	0.68

Light gray indicates an unsatisfactory performance, white indicates an average performance and dark gray indicates at least a good model performance.

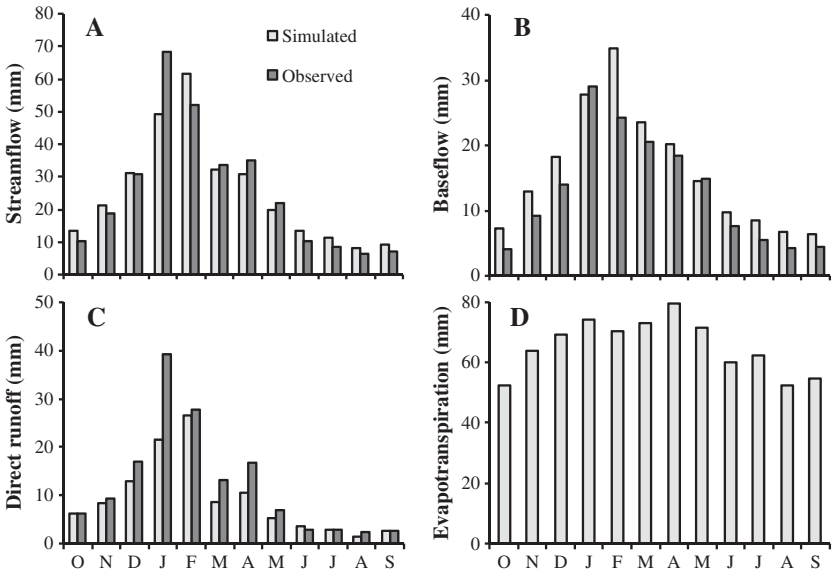

Figure 6. Comparisons of mean monthly observed and simulated (A) total streamflow, (B) baseflow, (C) direct runoff and (D) evapotranspiration at gauge S1. No observation of monthly ET was available for the study site

West Oahu (34%–79%) and Hawaii (33%–79%). Previous recharge estimates in terms of fraction of gross rainfall ranged between 18% and 43%, whereas the annual groundwater recharge accounts for 33% of the annual rainfall (Table V). The annual groundwater recharge in Hawaiian watersheds ranges between 18% and 43% of the annual rainfall, which indicates that the annual groundwater recharge of the current study fits well within the range of annual groundwater recharges reported for Hawaiian watersheds. This wide range of groundwater recharge on Hawaiian watershed is due to the spatial and temporal variability in rainfall across the landscape, which is influenced by the dominant impact trade winds (leeward vs. windward).

Hydrologic characteristics of the reference scenario

The mean monthly measured watershed rainfall varies between 49.6 mm in August and 178.3 mm in January (Table VI). The average monthly simulated streamflow at

S2 varied between 3.5 mm in August and 18.8 mm in January. Although the average annual rainfall is greater than 1000 mm, only 66% of the watershed receives more than 1000 mm of rain a year. The mean annual rainfall above gauge S1 was 1686 mm compared with 975 mm in the downstream area (between gauge S1 and S2). The minimum and the maximum monthly mean ET values were 49.8 mm in August and 74.6 mm in March, respectively. During the 43 years (1967–2009) of simulation period, the average annual precipitation, ET and streamflow varied between 1297, 766 and 122 mm, respectively (Table VII). Sixty-nine percent of the annual precipitation occurred during the wet season and the rest (31%) during the dry season. Seasonal variation of ET and streamflow were similar to that of rainfall.

Climate sensitivity of streamflow

The average annual and seasonal streamflow followed the precipitation dynamic under the current emission scenario (Table VII). However, the rates of increase and decrease in streamflow under increasing and decreasing precipitation scenarios were different (Figure 7A). The effect of precipitation changes on dry season streamflow was less pronounced than that of the wet season. An increase in the average air temperature by 1.1 and 6.4 °C decreased the annual streamflow by 0.5% and 2.6%, respectively. The −20% precipitation scenario resulted in a 50% decline in streamflow; however, a 20% increase in precipitation resulted in 72.8% increase in streamflow. The average rates of annual streamflow increase and decrease were 3.6 and 2.45 with each unit increase and decrease in precipitation, respectively (Figure 7A). As expected, the sensitivity of annual streamflow to precipitation decreased with increasing temperature. The effect of increasing temperature was more prominent under increasing precipitation scenarios. A 1.1 °C increase of the average temperature resulted in an annual streamflow decrease of approximately 0.9% in April and 0.07% in August. A 6.4 °C temperature increase resulted in a streamflow decrease of 3.89% in May and 0.40% in August. Effects of increasing and decreasing precipitation on streamflow were relatively small during the late summer (August, September and October) and highest during the late winter (February, March and April).

The changes in precipitation under B1 emission scenario did not alter the trend in the annual and seasonal streamflow as compared with those of the current emission scenario (Table VII). A maximum increase (71.4%) and decrease (50.2%) in annual streamflow, relative to the reference scenario, were the result of a 20% increase and decrease in the reference precipitation, respectively. Changes in leaf conductance and LAI had non-significant effects on annual streamflow (Table VIII). On the basis of paired *t*-test results, there was a non-significant ($p > 0.05$) difference between the percent change in the annual and the seasonal streamflow with and without changes in LAI and leaf conductance. Under B1 emission scenario, changes in annual and monthly mean streamflow due to changes in precipitation were similar to those of the current emission scenario. October had the smallest (42.98%) decrease and January had the largest increase (79.14%) in the mean monthly streamflow under 20% precipitation decrease and increase, respectively.

The sensitivity of annual and seasonal streamflow to changes in temperature and precipitation under the A1F1 emission scenario was more prominent compared with that of the current and B1 emission scenarios (Table VII). The paired *t*-test results show significant ($p < 0.001$) differences in annual and seasonal streamflow changes under the A1F1 and the current emission scenarios. Although the streamflow variations followed those of the precipitation, the increased patterns were different from the decrease responses. When the precipitation was decreased by 20%, the decline in annual streamflow (51%) was slightly higher than those under the current (50%) and B1 emission scenarios (50.2%). Similarly, when precipitation increased by 20%, the 68% increase in annual streamflow was lower than that of the B1 (71.4%) and the current emission scenario (72.8%). The annual streamflow under the A1F1 scenario increased by 3.5% for a 1% precipitation increase but decreased by 2.4% for 1%

Table 5. Comparisons of the values of the water balance components of the current study and with those reported in the literature

Recharge (%)	Streamflow (%)	ET (%)	Study location	Reference
31	8	61	Western Oahu	Nicholas *et al.* (1996)
31–39	32	36–39	Kauai	Izuka *et al.* (2005)
34	16	50	Molokai	Shade (1997)
24	43	33	Kauai	Shade (1995)
40	15	45	Southern Oahu	Giambelluca (1983)
43	15	42	Southern Oahu	Shade and Nichols (1996)
18	–	–	Hawaii	Oki (2002)
–	–	40–51	Hawaii	Giambelluca *et al.* (2009)
–	–	79	Western Oahu	Takasaki (1971)
–	–	34	Western Oahu	Mink (1978)
–	–	59	Mākaha, Oahu	Lao (2002)
19–40[a]	5	54–75[a]	Central Oahu	Giambelluca and Oki (1987)
33	11	56	Mākaha, Oahu	This study

[a] Recharge and ET were calculated using hourly, daily and monthly time steps.

Table 6. Average monthly water budget components and mean air temperature for the 43-year reference scenario

Month\variable	Precipitation (mm)	ET (mm)	Streamflow (mm)	Temperature (°C)
January	178.3	71.0	18.8	21.0
February	150.8	66.9	18.5	20.7
March	141.6	74.6	14.7	21.1
April	96.3	74.5	11.0	21.4
May	76.0	65.7	7.9	22.4
June	52.7	58.4	4.9	23.2
July	51.0	57.5	4.0	23.9
August	49.6	49.8	3.5	24.0
September	63.6	52.9	4.0	24.0
October	110.8	56.3	6.7	23.7
November	153.0	67.2	14.0	23.0
December	171.8	71.5	13.9	21.9
Average	108.0	63.9	10.1	22.5

precipitation decrease. The effect of CO_2 level on LAI and leaf conductance under A1F1 emission scenario had significant effects on annual and seasonal streamflows (Table VIII). A 6.4 °C temperature increase under this scenario resulted in a 9.2% increase in the annual streamflow compared with a 2.6% decrease under the current emission scenario. Paired *t*-test results show a highly significant ($p < 0.01$) difference between the percent change in streamflow with and without changes in LAI and leaf conductance. The contrasting responses of streamflow under different emission scenarios are presented in Figure 7B.

Table 7. Percentage change in ET and streamflow (SF) during each climate change scenario compared with the reference scenario with corresponding changes in temperature (T), precipitation (P) and CO_2 concentration assuming that changes in CO_2 emission will not affect the LAI and leaf conductance

CO_2 concentration (ppm)	T (°C)	P (mm)			ET (mm)			SF (mm)		
		Annual	Wet	Dry	Annual	Wet	Dry	Annual	Wet	Dry
Reference scenario	22.5	1296.8	891.8	404.8	766.4	425.6	340.8	121.8	90.8	31.0
	T (°C)	P (%)[a]			ET (%)[a]			SF (%)[a]		
Current emission scenario										
330	1.1	0			0.5	0.8	0.2	−0.5	−0.6	0.0
330	6.4	0			2.0	3.2	0.6	−2.6	−2.5	−2.6
330	0	−5			−2.3	−1.6	−3.2	−14.6	−15.3	−12.4
330	0	−10			−4.7	−3.2	−6.6	−27.8	−28.9	−24.5
330	0	−20			−10.3	−7.2	−14.1	−50.0	−51.4	−45.8
330	0	5			2.1	1.4	3.0	16.3	16.9	14.5
330	0	10			4.1	2.7	5.9	33.8	35.1	29.9
330	0	20			7.7	5.0	11.1	72.8	76.2	62.9
B1 emission scenario										
550	1.1	0			0.5	0.8	0.2	−0.5	−0.6	0.0
550	1.1	−5			−1.8	−0.8	−3.0	−15.1	−15.8	−13.0
550	1.1	−10			−4.3	−2.5	−6.5	−28.3	−29.4	−25.3
550	1.1	−20			−9.9	−6.5	−14.1	−50.2	−51.7	−45.5
550	1.1	5			2.7	2.2	3.3	15.4	16.0	13.7
550	1.1	10			4.7	3.5	6.2	32.8	34.1	28.9
550	1.1	20			8.4	5.9	11.4	71.4	74.8	61.7
A1F1 emission scenario										
970	6.4	0			2.0	3.2	0.6	−2.6	−2.5	−2.6
970	6.4	−5			−0.4	1.5	−2.8	−16.7	−17.4	−14.6
970	6.4	−10			−3.0	−0.3	−6.3	−29.5	−30.6	−26.4
970	6.4	−20			−8.8	−4.5	−14.2	−51.0	−52.4	−46.8
970	6.4	5			4.3	4.7	3.8	13.0	13.8	10.8
970	6.4	10			6.4	6.1	6.8	30.0	31.5	25.9
970	6.4	20			10.2	8.5	12.4	67.9	71.3	57.9
A1B emission scenario[b]										
330	0	−1.9	−5	5	0.1	−1.3	1.8	−6.7	−9.6	1.7
330	0	−5.3	−10	5	−1.1	−2.9	1.1	−17.2	−21.2	−5.3

[a] Percentage changes are relative to reference scenario;
[b] Scenarios based on Timm and Diaz (2008)

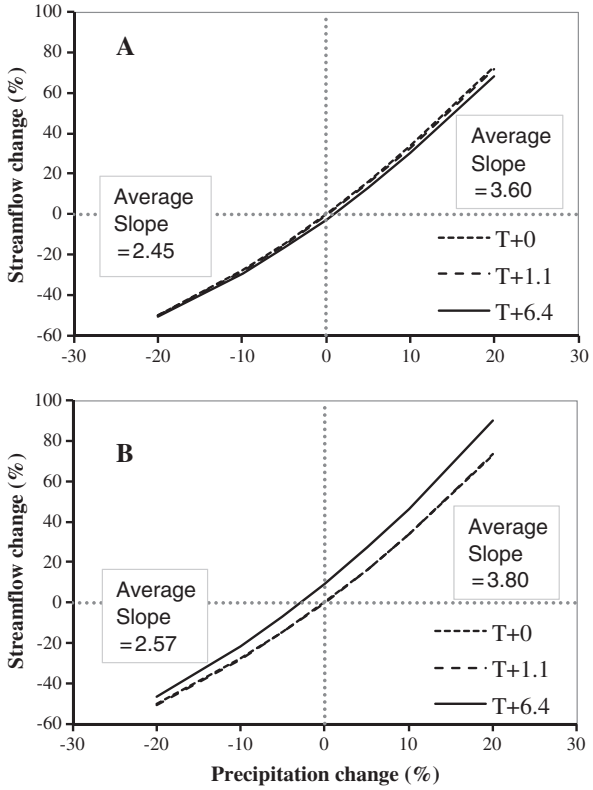

Figure 7. Streamflow changes in response to changes in precipitation and temperature without (A) and with (B) CO_2 effect on LAI and leaf conductance

Both scenarios of seasonal precipitation change under A1B emission scenario (−5 in wet and 5 in dry season and −10 in wet and 5 in dry season) resulted in decreased annual streamflow by 6.7% and 17.2% (Table VII). A decrease in the wet season precipitation and an increase in the dry season precipitation by 5% resulted in an increase in the streamflow during the month of July, August, September and October by 1.92%, 4.68%, 4.81% and 4.79%, respectively. During the remaining months of the year, the streamflow decreased with a maximum decrease rate of 12.08% in April and a minimum decrease rate of 0.09% in June. In the second scenario, when the wet season precipitation was decreased by 10% and the dry season precipitation was increased by 5%, the streamflow declined during all months except October, which showed a 1.4% increase in streamflow. The maximum streamflow decrease was 23.7% in April.

Climate sensitivity of evapotranspiration

Dry season ET was more sensitive to changes in precipitation compared with that of the wet season. However, the opposite was true with the increase in air temperature (Table VII). An increase in air temperature by 1.1 and 6.4 °C caused an increase in annual ET by 0.5 and 2%, relative to the reference scenario, respectively (Table VII). The sensitivity of ET to changing precipitation was similar to that of the streamflow. Changes in annual and seasonal ET decreased with increasing precipitation. A 1% decrease in precipitation caused 0.53% decline in annual ET compared with 0.39% when precipitation was increased by the same magnitude (Figure 8A). The largest increase in the annual ET was 7.7% with a 20% precipitation increase and the largest decrease was 10.3% with a 20% precipitation decrease. Changes in ET as a response to changes in temperature and precipitation varied by month. A 1.1 and 6.4 °C increase in temperature resulted in an increase in ET during all months except during late summer months where ET decreased relative to that of the reference scenario, indicating that most of the water was lost during the winter and early summer because of higher evaporative demand. Seasonality in ET was more prominent with precipitation scenarios. Decrease in ET during August and September was 75%–90% of the total decline in precipitation. The minimum and the maximum decrease in ET values with a 20% decrease in precipitation were 5.7% in January and 18.2% in August, respectively. However, the minimum and the maximum increase in ET values with a 20% increase in precipitation were 4.0% in January and 14.4% in August, respectively.

Changes in precipitation and temperature under B1 emission scenario caused ET to decline with a decreasing precipitation and to increase with an increasing precipitation. The ratio of change in annual ET per unit increase in precipitation was 0.39; however, this ratio was 0.52 for every unit decrease in precipitation. Average changes in annual ET during increasing and decreasing precipitations were similar to those of the current emission scenario. However, the sensitivity of annual ET to precipitation change during B1 and the current emission scenario was significantly different ($p = 0.002$). A 20% increase in precipitation under B1 emission scenario resulted in an 8.4% increase in annual ET compared with a 7.7% increase during the current emission scenario. The effect of CO_2 on LAI and leaf conductance resulted in a relatively smaller change in ET values (Table VIII) compared with those of the scenarios without modified LAI and leaf conductance (Table VII). Modified LAI and leaf conductance had greater impact on the wet season ET compared with that of the dry season. Changes in annual and seasonal ET with and without changes in LAI and leaf conductance were statistically significant ($p < 0.02$). The effect of modified LAI and leaf conductance was prominent with increasing precipitation scenarios (Figure 8B). Seasonal changes under this scenario were slightly different from the current emission scenario. An increase of temperature by 1.1 °C resulted in a decrease in ET during all months except July, August and September. The maximum and the minimum decreases in ET with a 20% precipitation decrease were 16.4% and 6.9% in August and January, respectively. A 20% precipitation increase resulted in a maximum and minimum increase in ET by 15.2% in August and 2.4% in February, respectively.

The effect of an increase in temperature and precipitation under A1F1 emission scenario caused a relative increase in ET for all precipitation scenarios (Table VII). Under decreasing precipitation scenarios, the annual and seasonal ET declined in all cases; however, the magnitude of decline was small compared with that of B1 emission

Table 8. Percentage change in ET and streamflow (SF) during each climate change scenario compared with the reference scenario with corresponding changes in temperature (T), precipitation (P) and CO_2 concentration. LAI and leaf conductance were modified to reflect the increase in CO_2 concentration

CO_2 concentration (ppm)	T (°C)	P (mm)			ET (mm)			SF (mm)		
		Annual	Wet	Dry	Annual	Wet	Dry	Annual	Wet	Dry
Reference Scenario	22.5	1296.8	891.8	404.8	766.4	425.6	340.8	121.8	90.82	31.03
	T (°C)	P (%)[a]			ET (%)[a]			SF (%)[a]		
Current emission scenario										
330	1.1	0			0.5	0.8	0.2	−0.5	−0.6	0.0
330	6.4	0			2.0	3.2	0.6	−2.6	−2.5	−2.6
330	0	−5			−2.3	−1.6	−3.2	−14.6	−15.3	−12.4
330	0	−10			−4.7	−3.2	−6.6	−27.8	−28.9	−24.5
330	0	−20			−10.3	−7.2	−14.1	−50.0	−51.4	−45.8
330	0	5			2.1	1.4	3.0	16.3	16.9	14.5
330	0	10			4.1	2.7	5.9	33.8	35.1	29.9
330	0	20			7.7	5.0	11.1	72.8	76.2	62.9
B1 emission scenario										
550	1.1	0			−0.9	−1.4	−0.3	−0.3	−0.4	0.0
550	1.1	−5			−3.1	−2.9	−3.4	−14.9	−15.6	−12.9
550	1.1	−10			−5.5	−4.5	−6.6	−28.3	−29.5	−24.7
550	1.1	−20			−10.9	−8.4	−14.0	−50.5	−52.0	−45.9
550	1.1	5			1.2	0.0	2.6	16.3	16.8	14.6
550	1.1	10			3.1	1.3	5.4	33.7	35.0	29.7
550	1.1	20			6.6	3.6	10.4	73.1	76.3	63.6
A1F1 emission scenario										
970	6.4	0			−9.4	−12.4	−5.7	9.2	8.5	11.1
970	6.4	−5			−11.2	−13.6	−8.1	−7.1	−8.3	−3.5
970	6.4	−10			−13.0	−14.9	−10.7	−21.7	−23.5	−16.5
970	6.4	−20			−17.3	−18.0	−16.4	−46.3	−48.3	−40.4
970	6.4	5			−7.8	−11.3	−3.5	27.2	27.2	26.9
970	6.4	10			−6.3	−10.2	−1.4	46.5	47.3	43.8
970	6.4	20			−3.6	−8.3	2.3	90.0	92.7	81.5

[a] Percentage changes are relative to reference scenario

scenario. Decrease in annual ET due to a decline of precipitation by 5% was nearly offset by a 6.4 °C increase in temperature. Changes in temperature and precipitation combined with modified LAI and leaf conductance for increased CO_2 concentration under A1F1 emission scenario resulted in a decreased ET for all precipitation scenarios (Table VIII). The largest decrease in annual ET was 17.3% for a 20% decline in precipitation, and the smallest decrease was 3.6% with a 20% precipitation increase. The rate of decrease in annual ET with decreasing precipitation scenarios was higher than that during increasing precipitation scenarios. An increasing and a decreasing precipitation by 1% resulted in a 0.29% and 0.40% decrease in annual ET, respectively. Increasing only temperature by 6.4 °C resulted in a 9.4% decline in annual ET. The contrasting climate sensitivity of annual ET under different CO_2 emission scenarios is illustrated in Figure 8B. ET decreased during all months in a response to decreasing precipitation scenarios with a maximum and a minimum decline in the months of May and September, respectively. There was an increase in ET during mid and late summer months under increased precipitation scenarios. The changes in ET were in the same direction as the changes in precipitation (i.e. an increase in precipitation caused an increase in ET and vice versa). The effect of modified leaf conductance and LAI on the sensitivity of annual and seasonal ET to changes in precipitation and temperature was statistically ($p < 0.001$) significant.

The effect of seasonal precipitation change scenarios had a very little effect on the annual ET but resulted in a significant change in seasonal ET (Table VII). Increasing and decreasing of the wet and dry season precipitation by 5% resulted in a 0.1% increase in the annual ET but a 1.8% increase during the dry season. However, decreasing the wet season precipitation by an additional 5% resulted in a 1.1% decline in annual ET and a maximum decline of 2.9% during wet season. Seasonal changes in ET were in agreement with seasonal changes in precipitation. The increase in ET during the summer months was smaller under the scenario with wet season precipitation declining by 10% compared with a 5% decline.

Climate elasticity of streamflow

The climate elasticity of streamflow was calculated with the nonparametric estimator of elasticity, which is based on the median of the ratio of the relative change in the model output to the relative change in the model input on a given time step (Sankarasubramanian *et al.*, 2001). Changes in

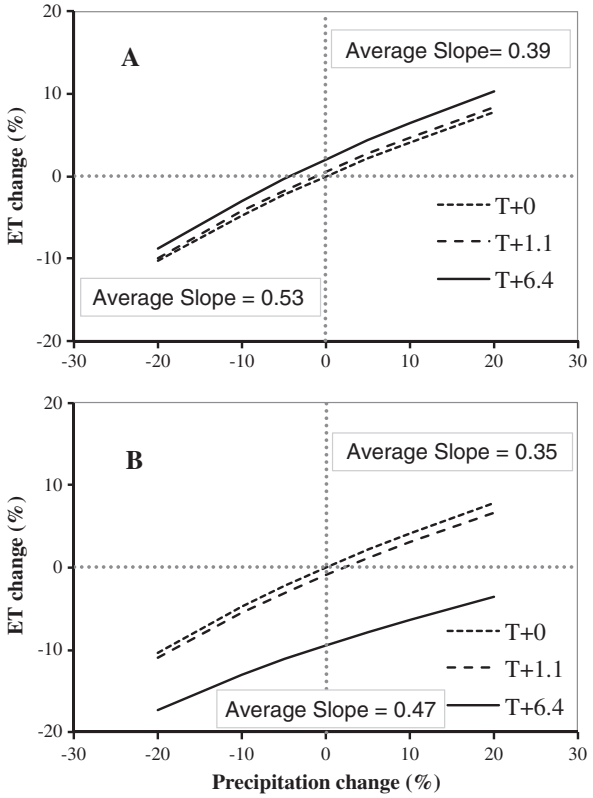

Figure 8. Evapotranspiration (ET) changes in response to change in precipitation and temperature without (A) and with (B) CO_2 effect on LAI and leaf conductance

streamflow as a function of temperature change showed a linear relationship for different precipitation scenarios (Figure 9). For a 20% precipitation increase, the slope of the streamflow–temperature curve was $-0.74\%\ ^{\circ}C^{-1}$, meaning that a 1 °C temperature increase will result in a 0.74% decrease in streamflow. However, for a 20% decrease in precipitation, the slope between streamflow and temperature was only $-0.16\%\ ^{\circ}C^{-1}$, indicating that streamflow will decline by only 0.16% per unit increase in temperature. This indicates that the streamflow is more sensitive to changes in temperature when it is combined with an increase in precipitation. If the precipitation were to remain constant, a 1 °C temperature increase will decrease the streamflow by a 0.40%.

The precipitation elasticity of streamflow increased with increasing precipitation. However, with increasing temperature, the precipitation elasticity of streamflow showed an increasing and decreasing trends under decreasing and increasing precipitation scenarios, respectively (Figure 9). The most significant change in the precipitation elasticity of streamflow was under 20% precipitation decline scenario, which increased from 1.84 at zero °C to 2.23 at 6.4 °C. As temperature increased, the difference in precipitation elasticities of streamflow under different precipitation scenarios decreased. A 2.3 precipitation elasticity of streamflow means that if the precipitation is changed by 1%, streamflow will change by 2.3%. The precipitation elasticity of streamflow results are consistent with the relative changes in streamflow for each precipitation change scenario reported in Table VII.

Climate elasticity of evapotranspiration

The changes in ET with increasing temperature showed linear increase for different precipitation scenarios (Figure 10). The maximum slope of the correlation between change in ET and temperature was ($0.38\ \%\ ^{\circ}C^{-1}$) associated with a 20% precipitation increase, whereas the minimum slope was ($0.22\ \%\ ^{\circ}C^{-1}$) with a 20% precipitation decrease scenario. The slope between ET and temperature was 0.31% $^{\circ}C^{-1}$ for unchanged precipitation scenario. As expected, the slopes of the ET–temperature relationship increased with increasing precipitation.

The precipitation elasticity of ET at 0 °C temperature change was the highest for 20% decreasing precipitation scenarios (Figure 10). For decreasing precipitation scenarios, the precipitation elasticity of ET decreased with increasing temperature. This trend was the opposite for increasing precipitation scenario where the precipitation elasticity of ET increased with increasing precipitation. At ~2 °C warming, the elasticity of ET under a 20% decline in precipitation was the same as for that of a 10% precipitation increase. Similarly, if the temperature is increased by ~2.75 °C, the elasticities of ET under a 10% decrease or a 20% increase in precipitation will be the same. Also, for a 6.4 °C warming, the elasticity of ET under a 20% increase or decrease of precipitation scenario is nearly the same. This clearly illustrates the nonlinearity in the sensitivity of ET to combined changes in precipitation and temperature.

DISCUSSION

The climate change scenarios were constructed using future emission scenarios based on the Fourth Assessment Report (AR4) and Special Report on Emission

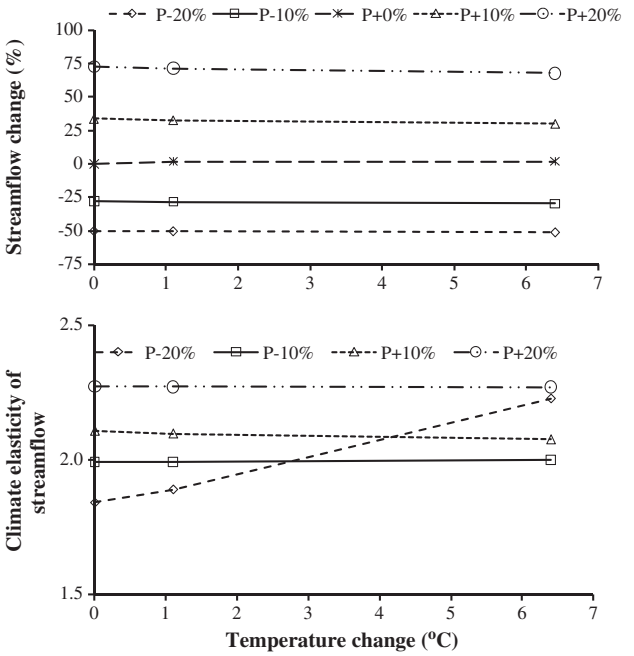

Figure 9. Streamflow change (top) and climate elasticity of streamflow (bottom) as a function of temperature change at different precipitation

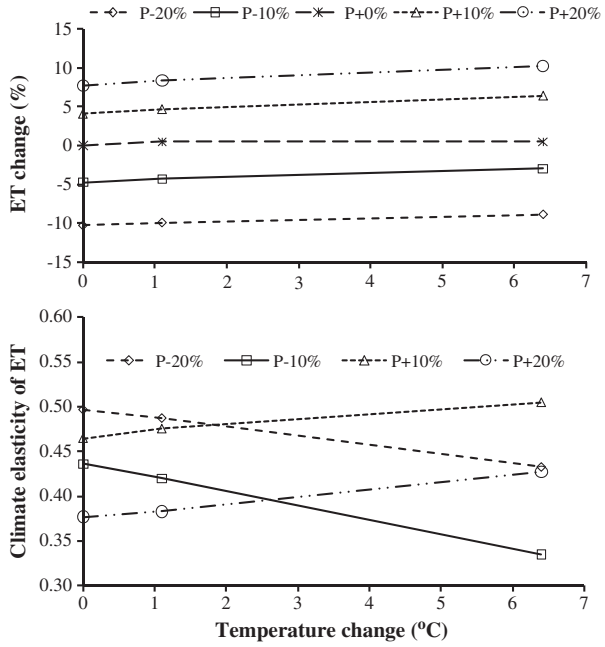

Figure 10. Changes in the ET (top) and climate elasticity of ET (bottom) as a function of temperature change at different precipitation

Scenarios of the IPCC in combination with the local trends in precipitation. However, potential uncertainty in the projections under each scenario remains, for example, the uncertainty in hydrologic predictions related to problem of equifinality in the model calibration (Sankarasubramanian *et al*., 2001). We used a very simple step change approach to simulate the effect of increased CO_2 on ET and streamflow. The potential feedback between vegetation, soil and atmosphere under elevated CO_2 (Smith and Shugart, 1993; Wang *et al*., 2006) was not accounted for. Although, the projected changes in ET and streamflow are subjected to the model uncertainty and validity of various climate change scenarios studied, they provide first-order vulnerability assessment. With all these uncertainties involved due to the complex and nonlinear nature of the system, the projected impacts should not be viewed as predictions, rather as a vulnerability analysis.

Elevated CO_2 emissions and changes in temperature and precipitation affected the streamflow as well as the ET of the study area. Effects of increased temperature alone on streamflow and ET were small compared with what was reported by other climate change studies (Fu *et al*., 2007; Ficklin *et al*., 2009; Liu and Cui, 2010). Absolute change in ET and streamflow with a 5% change in precipitation was higher than that due to a 6.4 °C increase in temperature, indicating that a 5% change in rainfall will have a more severe impact than a 6.4 °C increase in temperature alone. This could be attributed to an overall lower temperature during the year and a narrower amplitude (i.e. difference between daily minimum and maximum temperature) compared with the continental United States and other non-tropical climates around the world. In addition, because most of the rainfall in the leeward part of Hawaii occurs during the wet season, ET supply is limited during the dry season as it is shown from the combined temperature and precipitation effect on streamflow and ET. When changes in temperature are combined with those in precipitation, their impact on ET and streamflow is significant.

Increasing CO_2 concentration in the atmosphere would have a significant impact on ET and subsequently on streamflow especially under A1F1 emission scenario. We observed a significant decline in ET because of a decrease in leaf conductance with an increasing CO_2 concentration in the atmosphere. Higher antecedent soil moisture resulting from reduced transpiration could have been the reason behind the increase in streamflow. A similar response of elevated CO_2 concentration was reported by others studies (Eckhardt and Ulbrich, 2003; Ficklin *et al*., 2009). Because changes in the leaf conductance and LAI with increased CO_2 were solely based on values reported in the literature, extra care is needed in the interpretation of ET and streamflow changes. Although, changes in leaf conductance and LAI with changing CO_2 concentration in the atmosphere are highly variable and debatable, their impact on the hydrological components can be severe and hence should not be disregarded. Despite all the difficulties in transferring the greenhouse scale experimental results to field scale (Norby *et al*., 1999), a better assessment of forest response to increasing CO_2 is needed.

Sensitivity of streamflow to climate changes was slightly higher compared with what was reported by other studies (Fu *et al*., 2007; Ficklin *et al*., 2009; Gardner, 2009) with similar precipitation change. Streamflow is more sensitive to precipitation increase than to precipitation decrease. Results of decreasing precipitation scenarios are consistent with those of Tong and Liu (2006); however, changes in streamflow were higher under increasing precipitation scenarios. The higher sensitivity of streamflow to increasing precipitation can be attributed to the nature of the watershed. The watershed of this study is relatively small and highly mountainous (the average bed slope of the main stream above gauge S1 is 12.4%) as compared with watersheds in comparable studies. The time of concentration at S1 is only 0.41 hr and the time to peak is 0.38 hr (Wu, 1969). The less time of concentration will result in greater over land flow and less baseflow because it does not allow the soil to use full infiltration potential.

Although during the last 40 years the dominant vegetation in Mākaha watershed has not significantly changed (Mair and Fares, 2010a), recent eradication efforts of invasive species (e.g. strawberry guava) can also potentially alter the hydrology of the watershed. However, water resource development in the study area significantly affected the streamflow (Mair and Fares, 2010a; Safeeq, 2010; Mair and Fares, 2011). Current projected declines in streamflow (between 6.7% and 17.2%) under IPCC AR4 A1B are equivalent to those reported (11%–17%) by Mair and Fares (2010a) and Safeeq (2010) because of groundwater pumping since 1991.

SUMMARY AND CONCLUSION

A climate sensitivity of the main watershed hydrologic components (i.e. streamflow and ET) related to potential changes in CO_2 concentration, temperature and precipitation was performed in a flashy mountainous Hawaiian watershed using DHSVM. A total of 25 climate change scenarios were generated on the basis of the IPCC Special Report on Emission Scenarios and AR4 projections under current, B1, A1B1 and A1F1 emission scenarios. Under A1F1 emission scenario, the concentration of CO_2 in the atmosphere is expected to increase to a maximum of 970 ppm and the temperature by 6.4 °C. Precipitation changed by ±20% relative to the long-term mean monthly precipitation. Vegetation leaf conductance and LAI were modified to reflect the increase in CO_2 concentration. Simulations were performed for 43 years (1967–2009), and relative departures of streamflow and ET to the reference scenario were calculated on monthly, seasonal and annual scales.

Results of this study indicate that streamflow and ET are less sensitive to changes in temperature. However, when these changes are combined with changes in precipitation, they show a significant effect on all hydrological components of the watershed. The climate sensitivity of streamflow and ET to decreasing precipitation was higher than those during increasing precipitation scenarios. Changes in leaf conductance and LAI with increased CO_2 concentration had a significant effect on ET and subsequently on streamflow. The precipitation elasticity of ET and streamflow are lower and higher compared with other climate change sensitivity reported in other studies, respectively. Changes in precipitation would impact water quality more than changes in temperature would do. The finding of this study stresses the need for a more extensive assessment of the potential climate change impact on the hydrology of other Hawaiian watersheds.

ACKNOWLEDGMENTS

The project was partially supported by two grants from the US Department of Agriculture: (i) the Cooperative State Research, Education and Extension Service (grant no. 2004-34135-15058) and (ii) the McIntire-Stennis Formula (grant no. 2006-34135-17690). The authors also thank the Honolulu Board of Water Supply and members of the *Mohala I Ka Wai* for their assistance and cooperation.

REFERENCES

Alila Y, Beckers J. 2001. Using numerical modelling to address hydrologic forest management issues in British Columbia. *Hydrological Processes* **15**(18): 3371–3387.

Allen MR, Ingram WJ. 2002. Constraints on future changes in climate and the hydrologic cycle. *Nature* **419**: 224–232.

Alo CA, Wang G. 2008. Hydrological impact of the potential future vegetation response to climate changes projected by 8 GCMs. *Journal of Geophysical Research* **113**(G3): G03011.

Alves de Sena JO, Zaidan HA, Castro PRC. 2007. Transpiration and stomatal resistance variations of perennial tropical crops under soil water availability conditions and water deficit. *Brazilian Archives of Biology and Technology* **50**: 225–230.

Arnell NW. 1999. Climate change and global water resources—a new assessment. *Global Environmental Change* **9**(1): 31–49.

Arnold JG, Srinivasan R, Muttiah RS, Williams JR. 1998. Large area hydrologic modeling and assessment-Part I: model development. *Journal of American Water Resource Association* **34**(1): 73–89.

Beckers J, Alila Y. 2004. A model of rapid preferential hillslope runoff contributions to peak flow generation in a temperate rain forest watershed. *Water Resources Research* **40**: 1–19, W03501, doi:10.1029/2003WR002582.

Bonan GB. 2008. Forests and climate change: Forcings, feedbacks, and the climate benefits of forests. *Science* **320**(5882): 1444–1449.

Boorman DB, Sefton CEM. 1997. Recognizing the uncertainty in the quantification of the effects of climate change on hydrological response. *Climate Change* **35**: 415–434.

Breuer L, Eckhardt K, Frede HG. 2003. Plant parameter values for models in temperate climates. *Ecological Modelling* **169**(2–3): 237–293.

Bristow KI, Campbell GS. 1984. On the relationship between incoming solar radiation and daily maximum and minimum temperature. *Agricultural and Forest Meteorology* **31**: 159–166.

Burman R, Pochop LO. 1994. Evaporation, evapotranspiration and climatic data. Development of Atmospheric sciences, vol. **22**. Elsevier: Amsterdam, The Netherlands.

BWS. 2010. Watershed management plans, Available online: http://www.hbws.org/cssweb/display.cfm?sid=1406 (Accessed, 01/16/2010).

Canadell J, Jackson RB, Ehleringer JR, Mooney HA, Sala OE, Schulze ED. 1996. Maximum rooting depth of vegetation types at the global scale. *Oecologia* **108**(4): 583–595.

Chu PS, Chen H. 2005. Interannual and interdecadal rainfall variations in the Hawaiian Islands. *Journal of Climate* **18**: 4796–4813.

Chu PS, Chen YR, Schroeder T. 2010. Changes in precipitation extremes in the Hawaiian Islands in a warming climate. *Journal of Climate* **23**: 4881–4900.

Cordell S, Goldstein G, Mueller-Dombois D, Webb D, Vitousek PM. 1998. Physiological and morphological variation in *Metrosideros polymorpha*, a dominant Hawaiian tree species, along an altitudinal gradient: the role of phenotypic plasticity. *Oecologia* **113**: 188–196.

Cosgrove B, Rodell M. 1999. Land data assimilation systems vegetation parameters mapped to UMD classification scheme. National Aeronautics and Space Administration Goddard Space Flight Center, Greenbelt, MD. Retrieved from: http://ldas.gsfc.nasa.gov/LDAS8th/MAPPED.VEG/LDASmapveg.shtml [accessed: 26 Aug 2009].

Cuo L, Giambelluca TW, Ziegler AD, Nullet MA. 2006. Use of the distributed hydrology soil vegetation model to study road effects on hydrological processes in Pang Khum Experimental Watershed, northern Thailand. *Forest Ecology and Management* **224**(1–2): 81–94.

Cuo L, Lettenmaier DP, Alberti M, Richey JE. 2009. Effects of a century of land cover and climate change on the hydrology of the Puget Sound basin. *Hydrological Processes* **23**(6): 907–933.

Dickinson RE, Henderson-Sellers A, Kennedy PJ, Wilson MF. 1986. Biosphere Atmosphere Transfer Scheme (BATS) for the NCAR Community Climate Model, NCAR Technical Note NCAR/TN-275 + STR. National Center for Atmospheric Research, Atmospheric Analysis and Prediction Division, Boulder, CO [Also In: Gash, J.H.C. & Shuttleworth, W.J., 2007. Evaporation, IAHS Benchmark Papers in Hydrology Series,No. 2 pp. 410–486]. 69 pp.

Drake BG, Gonzàlez-Meler MA, Long SP. 1997. More efficient plants: a consequence of rising atmospheric CO_2? *Annual Review of Plant Biology* **48**(1): 609–639.

Easterling WE, Rosenberg NJ, McKenney MS, Allan Jones C, Dyke PT, Williams JR. 1992. Preparing the erosion productivity impact calculator (EPIC) model to simulate crop response to climate change and the direct effects of CO_2. *Agricultural and Forest Meteorology* **59**: 17–34.

Eckhardt K, Ulbrich U. 2003. Potential impacts of climate change on groundwater recharge and streamflow in a central European low mountain range. *Journal of Hydrology* **284**: 244–252.

ESRI I. 2006. ESRI ArcMap 9.2. ESRI, Iowa State Press: Redlands, California.

Ficklin DL, Luo Y, Luedeling E, Zhang M. 2009. Climate change sensitivity assessment of a highly agricultural watershed using SWAT. *Journal of Hydrology* **374**(1–2): 16–29.

Field CB, Jackson RB, Mooney HA. 1995. Stomatal responses to increased CO_2: implications from the plant to the global scale. *Plant, Cell & Environment* **18**: 1214–1225.

Fu G, Charles SP, Chiew FHS. 2007. A two-parameter climate elasticity of streamflow index to assess climate change effects on annual streamflow. *Water Resources Research* **43**(11): W11419.

Gardner LR. 2009. Assessing the effect of climate change on mean annual runoff. *Journal of Hydrology* **379**(3–4): 351–359.

Giambelluca TW. 1983. Water balance of the Pearl Harbor-Honolulu Basin, Hawai'i, 1946–75. University of Hawaii Water Resources Research Center Technical Report no., 151: 151.

Giambelluca TW. 1986. Land use effects on the water balance of a tropical island. *National Geographic Research* **2**: 125–151.

Giambelluca TW, Luke MSA. 2007. Climate change in Hawai'i's mountains. mountain views: The newsletter of the consortium for integrated climate research in western mountains. *Consortium for Integrated Climate Research in Western Mountains* **2**: 13–17.

Giambelluca TW, Oki DS. 1987. Temporal disaggregation of monthly rainfall data for water balance modelling. The Influence of Climate Change and Climatic Variability on the Hydrologic Regime and Water Resources (Proc. Vancouver Symp., Aug. 1987), 255–267. IAHS Publ. no. 168.

Giambelluca TW, Diaz HF, Luke MSA. 2008. Secular temperature changes in Hawai'i. *Geophysical Research Letters* **35**: L12702, doi:10.1029/2008GL034377.

Giambelluca TW, Martin RE, Asner GP, Huang M, Mudd RG, Nullet MA, DeLay JK, Foote D. 2009. Evapotranspiration and energy balance of native wet montane cloud forest in Hawai'i. *Agricultural and Forest Meteorology* **149**: 230–243.

Giambelluca TW, Nullet MA, Schroeder TA. 1986. Rainfall atlas of Hawai'i: State of Hawaii. Department of Land and Natural Resources Report R76: 267.

Gingerich SB, Oki DS. 2000. Groundwater in Hawai'i. U.S. Geological Survey Fact Sheet.

Groisman PY, Knight RW, Karl TR, Easterling DR, Sun B, Lawrimore JH. 2004. contemporary changes of the hydrological cycle over the contiguous United States: Trends derived from in situ observations. *Journal of Hydrometeorology* **5**(1): 64–85.

Gupta HV, Sorooshian S, Yapo PO. 1999. Status of automatic calibration for hydrologic models: Comparison with multilevel expert calibration. *Journal of Hydrologic Engineering* **4**: 135.

Hamlet AF, Lettenmaier DP. 1999. Effects of climate change on hydrology and water resources of the Columbia River basin. *Journal of the American Water Resources Association* **35**: 1597–1624

Hansen J, Sato M, Ruedy R, Lo K, Lea DW, Medinaelizade M. 2006. Global temperature change. *Proceedings of the National Academy of Sciences of the United States of America* **103**: 14 288–14 293.

Harman M. 2006. Mapping invasive species in Makaha valley, Oahu using fine resolution satellite imagery. Bachelor's Thesis, University of Hawaii at Manoa.

IPCC. 2001. Special Report on Emissions Scenarios (SRES). A Special Report of Working Group III of the Third Assessment Report of the Intergovernmental Panel on Climate Change. Nakicenovic N, Swart R (eds). Cambridge University Press: Cambridge, United Kingdom, 612 pp.

IPCC. 2007. Climate Change 2007: The Physical Science Basis. Contribution of Working Group I to the Fourth Assessment Report of the Intergovernmental Panel on Climate Change [Solomon, S., D. Qin, M. Manning (eds)]. Cambridge University Press: Cambridge, United Kingdom and New York, USA.

Izuka SK, Oki DS, Chen C. 2005. Effects of irrigation and rainfall reduction on ground-water recharge in the Lihue Basin, Kauai Hawaii. US Geological Survey Scientific Investigations Report 2005–5146, 48.

Karl TR, Knight RW, Easterling DR, Quayle RG. 1996. Indices of climate change for the United States. *Bulletin of the American Meteorological Society* **77**: 279–292.

Labat D, Godderis Y, Probst JL, Guyot JL. 2004. Evidence for global runoff increase related to climate warming. *Advances in Water Resources* **27**(6): 631–642.

Lao C. 2002. Hydrogeology of the Watersheds of Makaha Valley and Waianae Valley. Unpublished report, Honolulu Board of Water Supply.

Legesse D, Vallet-Coulomb C, Gasse F. 2003. Hydrological response of a catchment to climate and land use changes in Tropical Africa: case study South Central Ethiopia. *Journal of Hydrology* **275**(1–2): 67–85.

Lettenmaier DP, Wood AW, Palmer RN, Wood EF, Stakhiv EZ. 1999. Water resources implications of global warming: A U.S. regional perspective. *Climate Change* **43**: 537–579.

Liu Q, Cui B. 2010. Impacts of climate change/variability on the streamflow in the Yellow River Basin, China. *Ecological Modelling* **222**(2): 268–274.

Long SP, Ainsworth EA, Rogers A, Ort DR. 2004. Rising atmospheric carbon dioxide: plants face the future. *Annual Review of Plant Biology* **55**: 591–628.

Mair A, Fares A. 2010a. Influence of groundwater pumping and rainfall spatio-temporal variation on streamflow. *Journal of Hydrology* **393**(3–4): 287–308.

Mair A, Fares A. 2010b. Throughfall characteristics in three non-native Hawaiian forest stands. *Agricultural and Forest Meteorology* **150**(11): 1453–1466.

Mair A, Fares A. 2010c. Assessing rainfall data homogeneity and estimating missing records in Makaha valley, O`ahu, Hawai`i. *Journal of Hydrologic Engineering* **15**(1): 61–66.

Mair A, Fares A. 2011. Time series analysis of daily rainfall and streamflow in a volcanic dike-intruded aquifer system, O'ahu, Hawa 'i, USA. *Hydrogeology Journal* **1–16**, DOI 10.1007/s10040-011-0740-3.

Medlyn BE, Barton CVM, Broadmeadow MSJ, Ceulemans R, De Angelis P, Forstreuter M, Freeman M, Jackson SB, Kellomaki S, Laitat E, Rey A, Roberntz P, Sigurdsson BD, Strassemeyer J, Wang K, Curtis PS, Jarvis PG. 2001. Stomatal conductance of forest species after long-term exposure to elevated CO_2 concentration:1 a synthesis. *New Phytologist* **149**: 247–264.

Milly PCD, Dunne KA. 2001. Trends in evaporation and surface cooling in the Mississippi River basin. *Geophysical Research Letters* **28**(7): 1219–1222.

Mink JF. 1978. Waianae water development study, Honolulu Board of Water Supply 109 p., 6 appendices.

Mishra V, Cherkauer KA, Niyogi D, Lei M, Pijanowski BC, Ray DK, Bowling LC, Yang G, 2010. A regional scale assessment of land use/land cover and climatic changes on water and energy cycle in the upper Midwest United States. *International Journal of Climatology* **30**(13): 2025–2044.

Morison JIL. 1987. Intercellular CO_2 concentration and stomatal response to CO_2. In Stomatal Function, Zeiger E, Cowan IR, Farquhar GD (eds). Stanford University Press: Stanford, USA, 229–251.

Nash JE, Sutcliffe JV. 1970. River flow forecasting through conceptual models. Part 1. A discussion of principles. *Journal of Hydrology* **10**: 282–290.

Nichols WD, Shade PJ, Hunt CD, Jr. 1996. Summary of the Oahu, Hawaii, regional aquifer system analysis, Part 1. Professional Paper 1412-A, U.S. Geological Survey, 61 pp.

Niyogi D, Xue Y. 2006. Soil moisture regulates the biological response of elevated atmospheric CO_2 concentrations in a coupled atmosphere biosphere model. *Global and Planetary Change* **54**(1–2): 94–108.

Norby RJ, Wullschleger SD, Gunderson CA, Johnson DW, Ceulemans R. 1999. Tree responses to rising CO_2 in field experiments: implications for the future forest. *Plant, Cell & Environment* **22**(6): 683–714.

Oki DS. 2002. Reassessment of ground-water recharge and simulated groundwater availability for the Hawi area of North Kohala, Hawaii. US Geological Survey Water-Resources Investigations Report 02–4006, 62 p.

Oki DS. 2003. Surface water in Hawaii. U.S. Geological Survey Fact Sheet

Oki DS. 2004. Trends in streamflow characteristics in Hawaii, 1913–2003. U.S. Geological Survey Fact Sheet 2004–3104:4.

Oleson KW, Niu GY, Yang ZL, Lawrence DM, Thornton PE, Lawrence PJ, Stockli R, Dickinson RE, Bonan GB, Levis S. 2008. Improvements to the Community Land Model and their impact on the hydrological cycle. *Journal of Geophysical Research* **113**: G01021.

Pritchard SG, Rogers HH, Prior SA, Peterson CM. 1999. Elevated CO_2 and plant structure: a review. *Global Change Biology* **5**: 807–837.

Qi S, Sun G, Wang Y, McNulty SG, Myers JAM. 2009. Streamflow response to climate and landuse changes in a coastal watershed in North Carolina. *Transactions of the ASABE* **52**(3): 739–749.

Safeeq M. 2010. The response of different hydrologic processes under changing land use/land cover and climate in Mākaha watershed, O'ahu. Ph.D. thesis, University of Hawaii at Manoa, HI, USA.

Safeeq M, Fares A. 2011. Accuracy evaluation of ClimGen weather generator and daily to hourly disaggregation methods in tropical conditions. *Theoretical and Applied Climatology* 1–21.

Sankarasubramanian A, Vogel RM, Limbrunner JF. 2001. Climate elasticity of streamflow in the United States. *Water Resources Research* **37**(6): 1771–1781.

Santiago LS, Goldstein G, Meinzer FC, Fownes JH, Mueller-Dombois D. 2000. Transpiration and forest structure in relation to soil waterlogging in a Hawaiian montane cloud forest. *Tree Physiology* **20**(10): 673–681.

Saxe H, Ellsworth DS, Heath J. 1998. Trees and forest functioning in an enriched CO_2 atmosphere. *New Phytologist* **139**: 395–436.

Shade PJ. 1995. Water budget for the Island of Kauai, Hawaii. US Geological Survey Water-Resources Investigations Report 95–4128, 25.

Shade PJ. 1997. Water budget for the Island of Molokai, Hawaii. US Geological Survey Water-Resources Investigations Report 97–4155, 20.

Shade PJ, Nichols WD. 1996. Water budget and the effects of land-use changes on groundwater recharge, Oahu, Hawaii. Professional Paper 1412-C, U.S. Geological Survey, 38.

Smith TM, Shugart HH. 1993. The transient response of terrestrial carbon storage to a perturbed climate. *Nature* **361**: 523–526 doi:10.1038/361523a0.

Stratton L, Goldstein G, Meinzer FC. 2000. Stem water storage capacity and efficiency of water transport: their functional significance in a Hawaiian dry forest. *Plant, Cell & Environment* **23**(1): 99–106.

Takasaki KJ. 1971. Ground water in the Waianae District, Oahu, Hawaii. U.S. Geological Survey Hydrologic Investigations Atlas HA-358, 2 map sheets, scale 1:62,500.

Takasaki KJ, Mink JF. 1985. Evaluation of major dike-impounded ground-water reservoirs, island of Oahu. U.S. Geological Survey Water-Supply Paper 2217: 77.

Taub D. 2010. Effects of rising atmospheric concentrations of carbon dioxide on plants. *Nature Education Knowledge* **1**(8): 21.

Thanapakpawin P, Richey J, Thomas D, Rodda S, Campbell B, Logsdon M. 2007. Effects of landuse change on the hydrologic regime of the Mae Chaem river basin, NW Thailand. *Journal of Hydrology* **334**(1–2): 215–230.

Timm O, Diaz HF. 2008. Synoptic-statistical approach to regional downscaling of IPCC twenty-first-century climate projections: seasonal rainfall over the Hawaiian Islands. *Journal of Climate* **22**: 4261–4280.

Timm OE, Diaz HF, Giambelluca TW, Takahashi M. 2011. Projection of changes in the frequency of heavy rain events over Hawaii based on leading Pacific climate modes. *Journal of Geophysical Research* **116**: 12, doi:10.1029/2010JD014923

Tong STY, Liu AJ. 2006. Modelling the hydrologic effects of land-use and climate changes. *International Journal of Risk Assessment and Management* **6**(4–6): 344–368.

USDA-NRCS. 2008. (U.S. Department of Agriculture-Natural Resources Conservation Services) SSURGO soil Series Map of Oahu. Downloaded from http://datagateway.nrcs.usda.gov/.

USDC-NOAA, 2005. NOAA Coastal Services Center. (2001). Coastal Change Analysis Program. NOAA Coastal Services Center, Charleston.

Verger RP. 2008. Hawai'i's vanishing streamflows: A case study on the impact of groundwater pumping, rainfall, and vegetation changes on a streamflow in Hawai'i. MS Thesis, University of Twente, Enschede.

Wand SJE, Midgley GF, Jones MH, Curtis PS. 1999. Responses of wild C4 and C3 grass (Poaceae) species to elevated atmospheric CO_2 concentration: a meta-analytic test of current theories and perceptions. *Global Change Biology* **5**: 723–741.

Wang W, Anderson BT, Nathan Phillips N, Kaufmann RK. 2006. Feedbacks of vegetation on summertime climate variability over the North American grasslands. Part I: Statistical analysis. *Earth Interactions* **10**: 1–27.

Wigmosta MS, Lettenmaier DP, Vail LW. 1994. A distributed hydrology-vegetation model for complex terrain. *Water Resources Research* **30**(6): 1665–1679.

Wiley MW, Palmer RN. 2008. Estimating the impacts and uncertainty of climate change on a municipal water supply system. *Journal of Water Resources Planning and Management* **134**(3): 239–246.

Wu I. 1969. Hydrograph study and peak discharge determination of Hawaiian small watersheds: island of Oahu. Technical Report No. 30, Water Resources Research Center, University of Hawaii. 85.

Wullschleger SD, Gunderson CA, Hanson PJ, Wilson KB, Norby RJ. 2002. Sensitivity of stomatal and canopy conductance to elevated CO_2 concentration interacting variables and perspectives of scale. *New Phytologist* **153**: 319–331.

Yamamoto T. 1963. Soil moisture constants and physical properties ofselected soils in Hawaii. U.S. Forest Service Research Paper, PSW-P2.

Yoshitani J, Chen ZQ, Kavvas ML, Fukami K. 2009. Atmospheric model-based streamflow forecasting at small, mountainous watersheds by a Distributed Hydrologic Model: Application to a watershed in Japan. *Journal of Hydrologic Engineering* **14**(10): 1107–1118.

Zhao Q, Liu Z, Ye B, Qin Y, Wei Z, Fang S. 2009. A snowmelt runoff forecasting model coupling WRF and DHSVM. *Hydrology and Earth System Sciences* **13**: 1897–1906.

